ANALYSIS OF TWO-PHOTON POLYMERIZATION FOR THE DEVELOPMENT OF A RECONFIGURABLE MICRO-DEVICE MANUFACTURING SYSTEM

by

Serge L. Li Hoi Foo-Gregory

A dissertation submitted in partial fulfillment
of the requirements for the degree of
Doctor of Philosophy
(Mechanical Engineering)
in The University of Michigan
2012

Doctoral Committee:

Professor Elijah Kannatey-Asibu Jr., Chair
Professor Nikolaos Chronis
Professor Almantas Galvanauskas
Professor Jyotirmoy Mazumder

For my mother

ACKNOWLEDGEMENTS

Thank you so much to everyone. I would like to acknowledge all that have helped me on my journey.

I thank my academic advisor and committee chair, Professor Elijah Kannatey-Asibu Jr. for his constant and continued support and guidance in my academic endeavors. I thank all the members of my committee, Professors Nikolaos Chronis, Almantas Galvanauskas, and Jyoti Mazumder. I also thank Professor Yoram Koren, who recruited me to the University of Michigan from my undergraduate institution, Carnegie Mellon.

I am also greatly appreciative of other professors and staff who have provided support and guidance to me through the years: professor Jack Hu for master's research guidance and support into the PhD program, Julie DeFilipo and Tonya Marion for support with all lab and university related issues. Dr. John Nees, Professor Steven Yalisove, Professor John Whitaker, and Professor Roseanne Sension for their help with lab equipment and facilities.

Also, a big thank you to lab mates past and present, and all friends and family who have provided support in countless ways.

Thank you.

TABLE OF CONTENTS

LIST OF FIGURES

Figure

LIST OF APPENDICES

Appendix

ABSTRACT

ANALYSIS OF TWO-PHOTON POLYMERIZATION FOR THE DEVELOPMENT OF A RECONFIGURABLE MICRO-DEVICE MANUFACTURING SYSTEM

by

Serge L. Li Hoi Foo-Gregory

Chair: Elijah Kannatey-Asibu Jr.

Two-photon polymerization combines the concepts of multi-photon absorption with polymerization of free radical polymerizable monomers. It can be used to fabricate a variety of polymeric micro-devices including micro-fluidic, biomedical, micro-optical, and micro-mechanical devices. A critical aspect of two-photon polymerization is the resolution of the process. This work provides an analysis of the two-photon polymerization process and a model which relates the process parameters to the volume element (voxel) polymerized during two-photon polymerization. The model assumes a Gaussian beam and the effects of beam power, lens parameters, and resin sensitivity are investigated. Experimental investigation was performed to validate the model and a sensitivity analysis was also performed, and the results show that the voxel diameter is more sensitive to changes in beam power and resin sensitivity than to changes in the incident beam diameter.

In addition, a methodology is developed that optimizes the laser path required to fabricate a three-dimensional microdevice that has been designed using CAD software. It is based on a modified greedy heuristic used in optimizing the Traveling Salesman Problem

to form a laser path that follows all mesh points used to create the part. Finally, to enhance manufacturing productivity, a technique is developed that is based on holography and will enable several components to be produced simultaneously.

To use two-photon polymerization fabrication as a viable manufacturing process, a reconfigurable manufacturing system was developed which works with a variety of optical elements as well as both amplified and oscillator-only femtosecond pulsed lasers. The analysis, methodology and reconfigurable manufacturing system presented in this work enables the use of two-photon polymerization in making microdevices for a range of commercial and future research applications.

CHAPTER I

Introduction

1.1 Introduction

Two-photon polymerization is a process by which one can create polymeric microdevices by tracing the focal point of a pulsed laser in liquid resin to polymerize and therefore produce a desired shape. Free form three dimensional microdevices can be created by this process with a resolution lower than the diffraction limit, *Houbertz et al.* (2003). Current production methods use a single focal point for solidifying the resin, *Maruo and Inoue* (2006); *Kawata et al.* (2001).

Microdevices have several applications from the medical field to the electronics industry in the form of micro-electro-mechanical systems (MEMS), for example, in lab-on-chip devices where micro fluidic channels are used to manipulate and examine small fluid samples *Weibel et al.* (2007). Building some of these devices by two photon polymerization permits greater freedom in the design of the microdevices than traditional 3-D lithography techniques. The two photon absorption phenomenon is used in the creation of microdevices by simply moving the focal point of a laser beam through a predefined spatial geometry to polymerize specially formulated resins. Making microdevices by two photon polymerization results in fine microdevices that are entirely plastic, which can be useful for medical devices where glass and metallic devices may be undesirable. Other applications of microdevices that can be built by two photon polymerization include optical data storage,

where characters can be written layer by layer in resin or special crystals *Day et al.* (1999); *Glezer et al.* (1996). Working microdevices that can be used in the field of microbiology for manipulating cells can also be made by two photon polymerization, for example a microfluidic chemostat which is used to grow and culture microbes on a micro-scale *Weibel et al.* (2007). With two photon polymerization's ability to build virtually any three dimensional polymeric micro-scale device, the applications for the devices are vast, and the potential for this fabrication process is being realized through the work of researchers over the past few years and the work presented in this thesis.

1.2 Literature Review

Two-photon absorption was first theorized in work by *Goeppert-Mayer* (1931); *Goeppert-Mayer and Born* (1931). It is defined as the simultaneous absorption of two or more photons via virtual states in the medium. When a photon is absorbed by a molecule, a virtual energy state may be created. Two photon absorption occurs if a second photon is then absorbed while this virtual state exists, Figure 1.1. Rather than the traditional mode of excitation of a molecule that involves a single photon (1PA), two photon absorption (2PA) uses multiple photons of a longer wavelength to change the energy state of the molecule. This requires a highly intense laser beam at the focal point. This is achieved using a high numerical aperture lens to produce a sharply focused beam, for example a 1.5 mW beam focused by a 0.9 NA lens resulting in a $6.04 \times 10^9 W/m^2$ intensity at the focal point. With the appropriate photoinitiator, this creates a free radical that can be used in free radical polymerization.

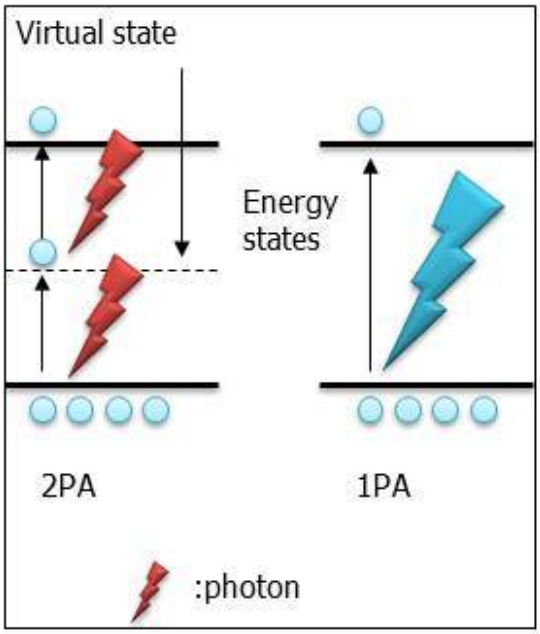

Figure 1.1: Schematic representation of two photon absorption and one photon absorption

Two-photon polymerization has been shown as a viable method for fabricating three dimensional microdevices *Galajda and Ormos* (2001); *Sun et al.* (2000); *Serbin et al.* (2004); *Kawata et al.* (2001); *Wu et al.* (2006); *Maruo and Inoue* (2006). Work has also been done on optimizing photoinitiators for two-photon polymerization *Kuebler et al.* (2001), as well as using the two-photon process for imaging and diagnosing the solidified microstructures *Sun et al.* (2001b); *Kawata and Sun* (2003). From previous work *Sun et al.* (2003); *Kawata et al.* (2001); *Honegger et al.* (2011), experimental results of voxel dimensions have been determined for specific photopolymerizable resins and process conditions.

Research in the field of two-photon polymerization has addressed issues such as the use of different lasers and resins to achieve polymerization *Kuebler et al.* (2001, 2000); *Maruo* (1997); determining the relationship between laser power and volume element (voxel) size *Sun et al.* (1999); and the fabrication of different shapes and structures on a micro scale *Galajda and Ormos* (2001); *Kawata et al.* (2001). Equipment used for two photon polymerization is typically a Ti:Sapphire laser with wavelength output 775 nm, and 100 - 150

femtosecond pulse duration. The beam is focused by a lens, and the focal point is moved in a three-dimensional space in the liquid resin by computer controlled stages. The rate of two photon transition is, in general, extremely small. Therefore, the laser power density has to be extremely high, on the order of several kilowatts per meter squared in order to obtain two photon absorption. For this reason, mode-locked near-infrared (IR) lasers are normally used. To emit extremely high peak powers, the pulse duration is as short as 100 fs. A titanium sapphire (Ti:Sapphire) laser is one of the best lasers currently available for peak powers of several tens of kilowatts *Maruo and Kawata* (1998).

In two-photon polymerization, a photoinitiator creates free radicals that lead to polymerization of monomers in a resin at specific wavelengths of light. The free radicals are created when the photoinitiator absorbs two or more photons simultaneously, figure 1.1. Polymerization by two or multi-photon absorption differs from that of single-photon absorption in that polymerization only occurs at the focal point of the light beam (from a laser) instead of along the entire path of the beam of light. As a result, three dimensional structures can easily be created by moving the focal point in the resin, tracing the outline of the desired shape, figure 1.2.

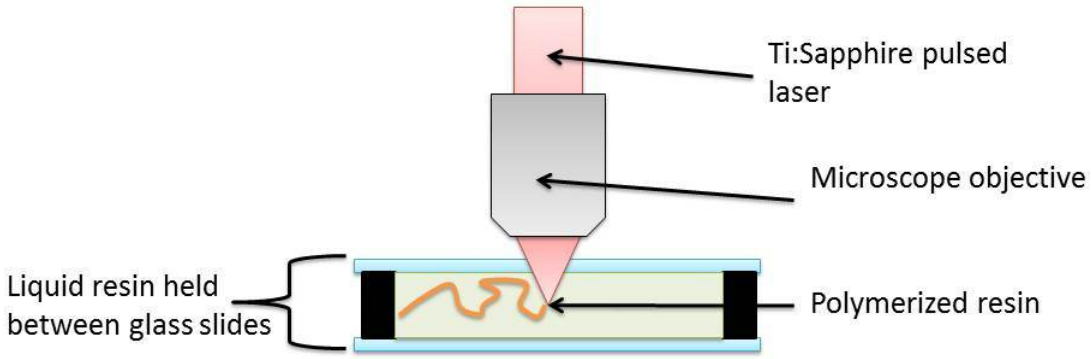

Figure 1.2: Polymerization along focal point traced path

Two-photon polymerization is a light intensity based process. Above the threshold intensity for polymerization (I_t), photoinitiators in the resin break down into free radicals to polymerize the monomer molecules in the resin. The process by which polymerization

occurs by two-photon absorption is outlined in chapter 2.

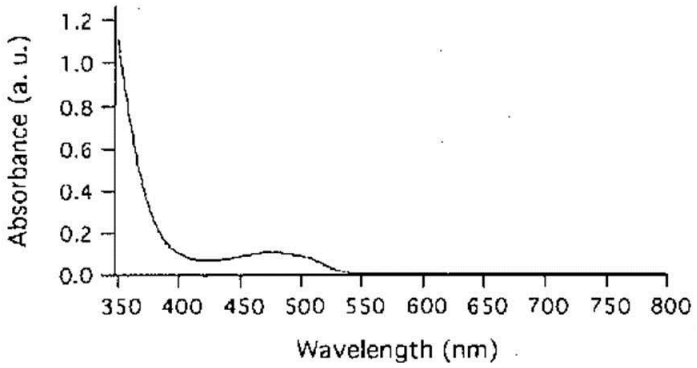

Figure 1.3: Absorbance vs. wavelength for SCR-500 resin *Maruo and Kawata* (1998)

Figure 1.3 illustrates the absorption band for a resin that is normally used in two photon polymerization. In the ultraviolet (UV) range, the resin absorbs the electromagnetic energy and polymerizes the liquid resin into solid. At the transmission wavelength of the Ti:Sapphire laser (775 *nm*), the resin does not absorb the energy, and so does not polymerize when exposed to 775 *nm* wavelength light. This essentially renders the liquid resin transparent to the laser at all positions except at the focal point of the laser, enabling three dimensional microdevices to be created within the bulk of the resin.

1.2.1 Two Photon Polymerization Resins

The key constituents of the resin used for two-photon polymerization are a photoinitiator and free radical polymerizable monomers, *Kuebler et al.* (2001). The photoinitiator is normally sensitive to the UV range of light and produces a free radical once excited by a suitable wavelength of light. At the focal point of the light source in the liquid resin, two photon absorption results in the effective wavelength of the light being cut in half. Thus when a 775 *nm* wavelength laser is used, the effective wavelength that induces two photon polymerization in the resin is 387.5 *nm* which is in the UV range of the spectrum. The chemical process for polymerization is terminated when all the free radicals produced by

the excited photoinitiator join chains of polymers or when the beam is moved or blocked *Maruo* (1997).

Photoinitiators include benzoyl chromophor (mixture of benzoyl cyclohexanol and morpholinophenyl amino ketones), which is sensitive to ultraviolet light and immune to infrared radiation. The most common commercially available resins used in two photon absorption thus far include SCR-500 from Japan Synthetic Rubber Company and Nopcocure 800 (NOP-800) from San Nopco. The SCR-500 resin, with an ultraviolet absorption band, is typically used with a Ti:Sapphire laser in the following operating mode: 790 *nm* oscillating wavelength, 200 fs pulse duration, 76 MHz, and 50 kW peak power. For the NOP-800 resin, which also has a single photon absorption band in the UV range, a laser of 400 *nm*, with 150 fs pulse duration, and 1 kHz repetition rate is typically used. Lenses with numerical aperture (NA) in the range of 0.85 to 1.4 are normally used to focus the beam. These lenses provide the small spot size required for fine feature detail in two-photon polymerization, and allow the use of low power high repetition rate lasers while still providing adequate intensity at the focal point. Commercially available photoinitiators and free radical polymerizable monomers from Sartomer, SR368, have also been used. Photoinitiators from Sartomer produce free radicals when exposed to light of wavelengths 200-400 nm. Figure 1.4 below is a graph of the isophores of a focused beam used in two photon polymerization, it shows the intensity distribution of the laser power in the focal region.

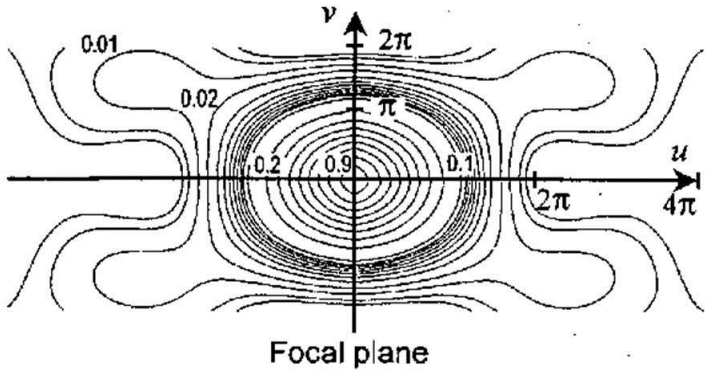

Figure 1.4: Isophores of the focused beam. Unitless parameters u and v are normalized axial (z) and lateral (r) coordinates *Sun et al.* (2002)

1.2.2 Voxel and Laser Relationship

A voxel is the smallest unit of solidified polymer that forms at the focal point of the light during two-photon polymerization. It can be smaller than the focal size of the laser light depending on the power used. The shape, size, and aspect ratio of the voxels depend on several factors including laser power, exposure time, and lens used. The correlation between the voxel size and exposure time is non-linear, Figure 1.5, and is normally determined experimentally. The voxel size determines the process resolution. Microfabrication with resolution three times smaller than the diffraction limit has been demonstrated *Sun et al.* (2002). The creation of microdevices using two photon absorption is done by moving the focal point of the laser beam from voxel to voxel to form the desired shape. Below is a graph and pictures demonstrating how the voxel size can be controlled with exposure time, the voxels are photographed from the side. The longer the exposure, the larger the voxel gets along the path of the laser beam.

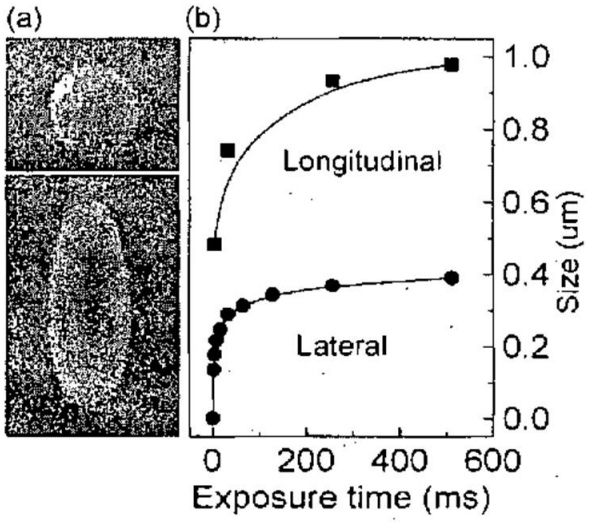

Figure 1.5: Graph of exposure time vs. voxel size. (a) SEM images of an isolated complete voxel, the 3D image of the TPE focal spot, (b) Variation of voxel size with exposure time. *Sun et al.* (2002)

The work of *DeVoe et al.* (2003) shows that it is possible to create voxels that have aspect ratios (depth to width ratio) from unity to as high as 8. Thus in creating microdevices by two photon polymerization, one must have precise control of laser power, exposure time, and speed of the moving focal point.

When the laser power is lower than the polymerization threshold ($(\text{TPA})_{TH}$), no polymerization will take place, and when the power is too high, the resin will boil. Experiments have shown that the relationship between laser power and voxel size for NOP resins is non-linear, Figure 1.6, and there exists a small power range for effective polymerization of the liquid resin *Sun et al.* (2000). Also, the graphs shows that there is a voxel size difference when the beam is moved in the $X-Y$ plane as opposed to vertically (Z direction).

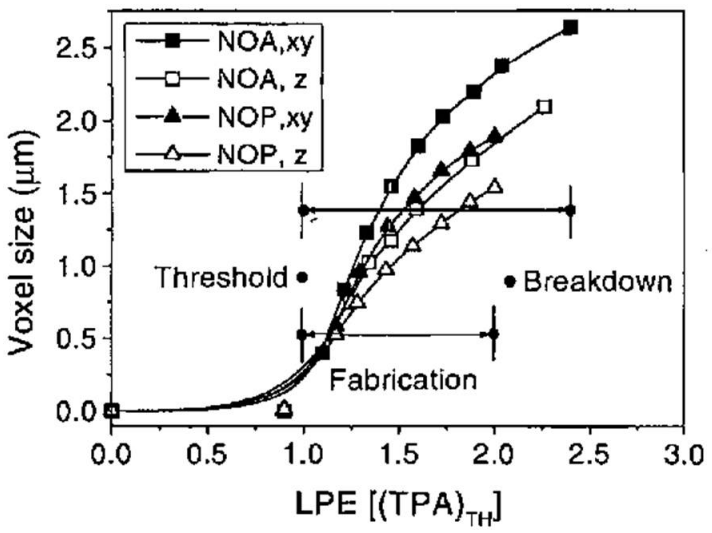

Figure 1.6: Graph of voxel size vs. input laser power, LPE: laser pulse energy, TPA: two photon absorption. LPE-dependent spatial resolutions of two kinds of resin. The data are from atomic-force microscope scanning of the solidified rods. The LPE's were normalized to the TPA exposure threshold of each resin. For NOP-800 and NOA-68, the values are (TPA)TH = 0.2 J and (TPA)TH = 0.5 J, respectively, *Kawata et al.* (2001)

Research has been done in the field of single-shot two-photon exposure to allow the resin to be excited by a single-shot from the laser, *Witzgall et al.* (1998). Optimizing the excitation wavelength for two photon absorption, it is possible to expose resin with a single shot from a Ti:Sapphire laser. This allows structures to be produced as fast as the repetition rate of the laser, 80 - 100 x 10^6 voxels/s. Thus writing of three dimensional structures is limited only by the ability to scan from voxel to voxel. Also with the energy available from Ti:Sapphire lasers, single-shot exposure should be possible for areas of the order of 1 mm^2, enabling the rapid production of large-scale devices, *Witzgall et al.* (1998). With single shot polymerization, one pulse from the laser is used to create a voxel. With multi-shot polymerization it may require hundreds or thousands of pulses from the laser to create a voxel. For single shot voxel creation the energy in a single laser pulse must be

above the minimum polymerization threshold to break down the photoinitiator and create the required free radical. It typically requires multi-shot exposure to form a voxel because the concentration of the photoinitiator is very low, less than 5%, and not every free radical formed will start a polymer chain. Usually more than 60% will start polymer chains. For single shot voxel creation to be effective, one needs to have several free radicals formed with every laser pulse so that polymer chains can be started and voxels created.

1.2.3 Microdevices Fabricated

Microdevices that have been fabricated by two photon polymerization include interlocking chain link, micro-bull, light driven propeller, and spring *Galajda and Ormos* (2001); *Kawata et al.* (2001); *Kuebler et al.* (2001). The micro-bull fabricated in one case is 10 μm by 7 μm (about the size of a human red blood cell), and required three hours to produce, figure 3.1.

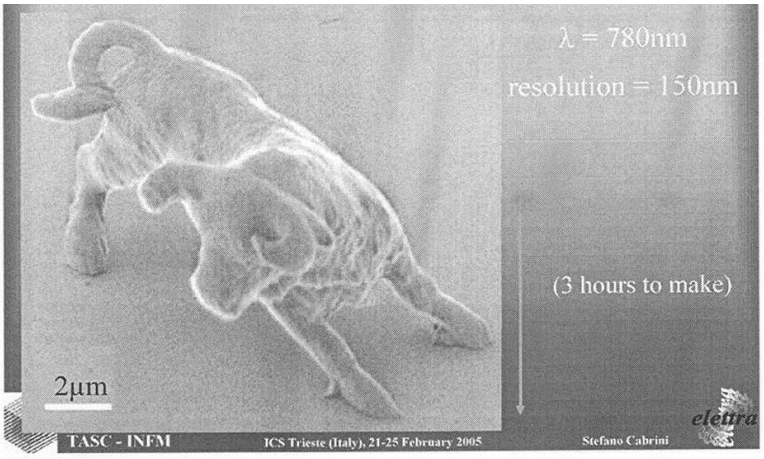

Figure 1.7: Micro-bull created by two-photon polymerization, *Kawata et al.* (2001)

A submicron oscillator, figure 1.8, was created to test the elastic force of solidified polymers and to determine the correlation between macro-scale physics and the properties of micro-scale structures created by two photon polymerization *Sun et al.* (2001a). With the submicron oscillator, a laser trapping force was used to extend the spring and determine the

stress-strain relationship. Using macro-scale physics, the expected spring rate was several magnitudes higher (order of $10^{-3}\ N/m$) than the spring rate determined experimentally (order of $10^{-6}\ N/m$). This difference in the calculated spring rate and the actual spring rate is due to the effects of atomic forces and surface phenomena dominating in the nano-scale devices.

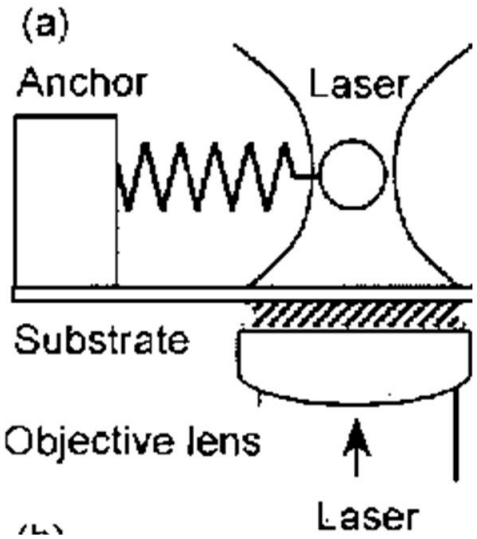

Figure 1.8: Micro-spring created by two-photon polymerization, *Sun et al.* (2001a)

Other interesting devices that have been made by two photon polymerization include a light driven propeller. In this case a shaft with blades was created by two-photon polymerization and by using light of different wavelengths than that used for the polymerization process, the device itself could be held and manipulated by light. In this case the shaft was connected to a series of cogs to demonstrate the ability to manipulate microdevices using only light, figure 1.9.

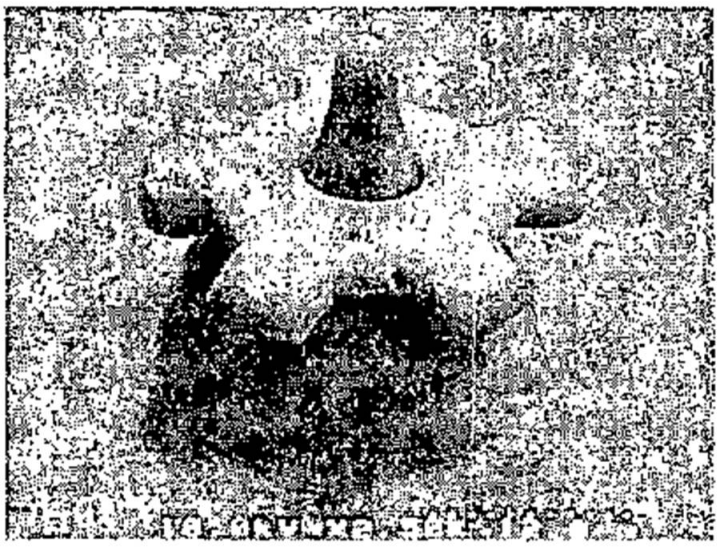

Figure 1.9: Freely moveable gear and shaft made by two-photon polymerization, *Sun et al.* (2000)

1.2.4 Optical Data Storage

Research in the area of optical data storage using two photon absorption focuses on the creation of shapes on different levels of resin and consequently reading the characters at each different level, figure 1.10. An example crystal used for this experiment was $LiNbO3$ (a photorefractive material).

Exposing certain organic polymers to two photon absorption changes the structure of the polymer itself, as opposed to polymerizing a liquid resin, at the focal point. The absorption spectra of the polymer is changed by two photon radiation causing a variation in the exposed material that can be visually detected, allowing for optical data storage.

Materials that can exist in different states and switch their isomer structure when exposed to different wavelength lights are said to be photochromic. These materials are used for optical data storage by creating physical differences between the exposed and unexposed regions, figure 1.10. Using two photon absorption, one is able to read back the data at different levels without interfering with data from other levels in the material, while also

being able to erase data by changing the isomer structure back to its original form. Again these materials only change their structure at the focal point of the laser and not along the beam, in the same way that two photon polymerization only takes place at the focal point.

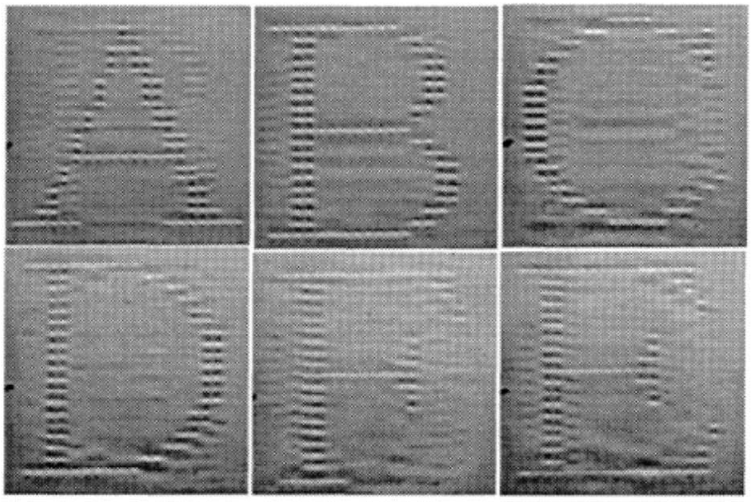

Figure 1.10: Letters of the alphabet drawn on different levels using two photon absorption *Kawata and Sun* (2003)

1.3 Research Objectives

The field of two photon polymerization is relatively young. Micro-devices developed by two-photon polymerization can be used in medical devices, and for integration into traditional MEMS fabrication devices. Models of the voxel size formulation are necessary to determine the process parameter to voxel formation relationship. The goal of this research is to investigate the potential for mass producing micro-components using two-photon polymerization. This involves:

1. Developing an analytical model to determine the relationship between process parameters and voxel formation.
2. Performing experiments to verify the analytic model and establish its validity.
3. Providing a methodology for creating micro-devices and optimizing the laser path.
4. Developing a reconfigurable manufacturing system for two-photon polymerization .

5. Demonstrating the applications and proposing future research directions.

The research that was undertaken to accomplish this goal is presented in the next chapters.

1.4 Dissertation Outline

This chapter provides a general background on the two-photon polymerization process, and discusses prior research in this area. In chapter II, an analytic model is developed that relates the voxel size to major process parameters such as power, focusing element, speed, and resin sensitivity. The model is validated by comparing the model predictions with experimental results, this work was been submitted to the ASME Journal of Micro and Nano-Manufacturing. Chapter III presents the methodology for creating microdevices by two-photon polymerization and an algorithm for optimizing the laser path needed for creating an object using a g-code, which also prevents the formation of unwanted features. Chapter IV investigates the potential for using holography to create objects by two-photon polymerization and thereby enhance productivity. Chapter V presents the hardware considerations and development of the reconfigurable manufacturing system for two-photon polymerization (RMS-TPP). Conclusions, research contributions, and future research directions are finally presented in chapter VI.

CHAPTER II

Analytic Model Formulation

Table of Variables

α	Beam attenuation in resin.
ϕ	Wave phase as a function of position z.
λ	Wavelength.
γ	Ray slope of wave $\gamma \approx \chi$ / R.
chi	Coordinate position of ray above optical axis.
Ψ	Amplitude distribution in a Gaussian wave.
ω	Frequency of light wave.
c	Speed of light.
D	Beam diameter.
f	Focal length.
I_f	Peak intensity at focal point.
I_p	Beam peak intensity.
$I_p(z)$	Beam peak intensity as a function of z.
I_t	Threshold intensity for polymerization.
$I(z,r)$	Beam intensity in axial and radial directions.

k	$k = \omega/c$, propagation constant or wave number.
k_p	Polymerization rate.
m	Polymerization rate factor.
P	Total beam power.
P_f	Beam power in focal region.
q	Complex curvature of a Gaussian beam.
$Q(z)$	Complex variable associated with reciprocal of Gaussian width.
r	Radial coordinate.
r_p	Radius of polymerized voxel.
$r_t(z)$	Radius of Gaussian beam over the minimum polymerization threshold at any position z.
R	Wave radius.
w_f	Beam radius at its waist.
$w(z)$	Beam radius as a function of position z.
x, y, z	Orthogonal 3-D coordinate directions.
Z_{max}	Calculated maximum voxel dimension in the z direction.

2.1 Introduction

Two-photon polymerization is a process for manufacturing polymeric microdevices using the tightly focused energy from a femtosecond pulsed infrared laser. The process combines the two-photon absorption and free radical polymerization phenomena. Two-photon absorption is a special case of multiphoton effects which were first theorized in work by *Goeppert-Mayer* (1931), *Goeppert-Mayer and Born* (1931). During two-photon polymerization, energy from multiple photons excites photoinitiators thereby emitting free radicals, which then polymerize monomers that are susceptible to free radical polymerization. Since a very high intensity source is essential for the two-photon absorption effect, it only takes place at the focal point, solidifying a volume element, or voxel, at this location. Three di-

mensional net-shape micro-devices can therefore be created in free form within the resin by tracing out the object features within the resin using the focal point. This contrasts with traditional lithographic rapid prototyping processes which require layer by layer processing, *Yamada et al.* (2007). Also differing from other light based micro-fabrication processes such as projection micro-fabrication, *Li-Hsin et al.* (2008); *Jae-Won et al.* (2009), which use masks to selectively polymerize the resin.

The process of two-photon polymerization is achieved through free radical polymerization of the liquid resin by a photolytic process. The photons from the light source excite the photoinitiator molecules in the resin, creating free radicals which initiate the polymerization process. These free radicals join the monomers in the liquid resin to form chain radicals that grow in length by adding monomers to the chain. Polymerization is ended when chain radical molecules join to form a molecule with no radical activity. The mechanism by which polymerization occurs by two photon absorption is outlined below, *Odian* (1970).

Let:

I: indicate the photoinitiator

R: free radical

M: monomer-oligomer

Mn: polymer

$R-(Mn)$: chained radical

hv: photon

$\bullet$: unpaired electron creating radical molecule

Initiation:

$$I + 2hv \rightarrow 2R\bullet$$

$$R\bullet + M \rightarrow RM\bullet$$

Propagation:

$$R-(Mn)_x\bullet + M \rightarrow R-(Mn)_{x+1}\bullet$$

Chained radical of length x + monomer $\rightarrow$ chained radical of length $x+1$

Termination:

$$-M\bullet + \bullet M- \rightarrow -M-M-$$

Two-photon polymerization has been shown as a viable method for fabricating three dimensional microdevices *Galajda and Ormos* (2001); *Sun et al.* (2000); *Serbin et al.* (2004); *Kawata et al.* (2001); *Wu et al.* (2006); *Maruo and Inoue* (2006). Work has also been done on optimizing photoinitiators for two-photon polymerization *Kuebler et al.* (2001), as well as using the two-photon process for imaging and diagnosing the solidified microstructures *Sun et al.* (2001b); *Kawata and Sun* (2003), and integrating two-photon polymerization with nanoimprinting *Zhang et al.* (2010). From previous work *Sun et al.* (2003); *Kawata et al.* (2001); *Honegger et al.* (2011), experimental results of voxel dimensions have been determined for specific photopolymerizable resins and process conditions. This thesis report presents an analysis of the two-photon polymerization process which enables the shape and size of the solidified volume element, the voxel, to be predicted. This is important in the design of microdevices that are to be fabricated by two-photon polymerization to control feature sizes, and later to produce larger devices more efficiently. Through this analysis and determination of expected voxel size one can better control the two-photon process based on the features desired in the microdevice. The voxel size determines the resolution of the

process. The beam and resin interaction is analyzed based on the input power, the lens used to focus the beam, and the threshold intensity required for polymerization. The intensity distribution of the beam is assumed to be Gaussian. The sensitivity of the polymerization process to each of the input factors is also analyzed.

2.2 Analysis

In this section the relationship between the voxel size and the beam peak intensity, total power, and minimum spot size at the focal point is developed.

From *Guenther* (1990) the basic Gaussian profile for a plane wave propagating in the z direction is:

$$\Psi = \left(\frac{w_f}{w(z)}\right) e^{\left(-\frac{r^2}{w(z)^2}\right)} e^{\left(-ik\frac{r^2}{2R(z)}\right)} e^{(-i\phi(z))} \tag{2.1}$$

This gives the intensity profile in the radial direction of a Gaussian beam at its focal position as, which will be used as the basis for power to intensity relationship developed later:

$$I(r) = I_p e^{\left(-\frac{r^2}{w_f^2}\right)} \tag{2.2}$$

For two-photon polymerization, the behavior of the beam in the neighborhood of the focal point is of utmost interest. To determine the beam radius at the focal point, we consider the radius to be equal to the beam waist after the lens, with the lens fully exposed by the beam, at a distance f from the lens. Thus we have, *Guenther* (1990):

$$w_f^2 = \frac{\frac{D^2}{4}}{\left[1 + \left(\frac{\pi D^2}{4\lambda f}\right)^2\right]} \tag{2.3}$$

The beam power is the product of the intensity and area at any section, and the power at the focal point, P_f, is equal to the incident power if the beam is not absorbed by the resin. Thus, from equation (2.2), the power, P_f , available to polymerize the resin at the focal

point can be expressed as:

$$P_f = I_f \int_{r=0}^{\infty} \int_{\theta=0}^{2\pi} e^{\left(-\frac{r^2}{w_f^2}\right)} r d\theta dr \tag{2.4}$$

$$= 2\pi I_f \int_{r=0}^{\infty} e^{\left(-\frac{r^2}{w_f^2}\right)} r dr \tag{2.5}$$

Now let:

$r^2 = v$, $2rdr = dv$

Then:

$$P_f = \pi I_f \int_{v=0}^{\infty} e^{\left(-\frac{v}{w_f^2}\right)} dv \tag{2.6}$$

Or

$$P_f = \pi I_f w_f^2 \tag{2.7}$$

A more general relationship between the beam power from the laser source and the peak intensity $I_p(z)$ for any position z along the beam can be shown [Appendix B] to be:

$$I_p(z) = \frac{P}{\pi w_f^2 \sqrt{1 + \left(\frac{\lambda z}{\pi w_f^2}\right)^2}} \tag{2.8}$$

The peak intensity of the Gaussian wave decreases with distance away from the focal point as the beam expands.

If we define the threshold intensity as the intensity level necessary to initiate polymerization, then the beam radius over which the resin is expected to be polymerized at the focal point is obtained by setting the threshold intensity equal to I in equation (2.2) and solving for the radius r_t, as:

$$I_t = I_f e^{\left(-\frac{r_t^2}{w_f^2}\right)} \tag{2.9}$$

Thus from equations (2.8) and (2.9), the threshold radius can be shown [Appendix C] to be:

$$r_t(z) = w(z)\sqrt{ln(I_p(z)) - ln(I_t) + ln\left(\frac{w_f}{w(z)}\right)} \tag{2.10}$$

However, polymerization most likely begins along the beam path before reaching the focal point and thus the beam is attenuated starting at Z_{max}, where the peak intensity is equal to the threshold intensity for polymerization.

The intensity distribution can then be expressed as:

$$I(z,r) = \frac{P}{\pi w_f w(z)}\left(\frac{w_f}{w(z)}\right) e^{\left(\frac{-r^2}{w(z)^2}\right)} e^{-\alpha(Z_{max}-z)} \tag{2.11}$$

Where $z \leq Z_{max}$.

$$Z_{max} = \frac{\sqrt{P^2 - I_t^2 w_f^4 \pi^2}}{I_t \lambda} \tag{2.12}$$

We now take into account the time dependence of polymerization, and consider the radius r_p which accounts for the voxel growth during polymerization. Assuming a circular voxel cross-section, the area polymerized at any section is given by:

$$A = \pi r_p(z)^2 = A_0 + k_p t \tag{2.13}$$

where A_0 is the area polymerized instantaneously at the time $t = 0$, with a radius of r_t, k_p is the polymerization rate, and t is the exposure time. Therefore, the voxel radius as a function of polymerization rate and time of exposure is given by:

$$r_p = \sqrt{\frac{A_0 + k_p t}{\pi}} \tag{2.14}$$

Further assuming a linear relationship between polymerization rate and intensity above the threshold I_t as demonstrated by Kuebler *Kuebler et al.* (2001), k_p can be expressed as:

$$k_p = [I(r,z) - I_t]\, m \tag{2.15}$$

where m = polymerization rate constant. In Kuebler's work, m was determined experimentally.

Combining equations (2.11), (2.14), and (2.15) yields the voxel radius at every position along the beam where the intensity is adequate for polymerization. This is given [Appendix D] by:

$$r_p(z) = \sqrt{\frac{A_0 + \left[\frac{P}{\pi w_f w(z)} \left(\frac{w_f}{w(z)}\right) e^{\left(\frac{-r^2}{w(z)^2}\right)} e^{-\alpha(Z_{max}-z)} - I_t\right] mt}{\pi}} \tag{2.16}$$

In this equation, z = 0 at the focal point.

Equation (2.16) shows that the voxel radius at any section increases as the square root of the laser power. However, this relationship may only be valid as long as there are photoinitiators available for polymerization. At high enough powers, the resin becomes saturated when all the available photoinitiators in the focal region are used up, and no more are available to start new polymer chains. This upper limit of the laser power depends on the initiator concentration, and can be obtained by estimating the number of photoinitiators in the focal region, and comparing with the number of photons in the focal volume. The number of photoinitiator molecules is then the product of the initiator concentration in the resin and the focal volume.

2.3 Description of Experiments

Creating a microdevice by two-photon polymerization involves moving the focal point of a laser beam to trace the object volume. Because the laser is a pulsed system, multiple pulses are exposed to each region as the focal point moves, allowing the formation of a continuous solid structure. If motion of the focal point were to be increased to the point where the pulses did not overlap, then individual voxels could be formed. In this experiment, the focal point position was controlled in the horizontal plane by a set of orthogonal linear motion stages with a resolution of 0.005 μm for each axis, and the vertical position was controlled by moving the focusing element as shown in figure 2.1 below, also with a 0.005 μm resolution along the z-axis.

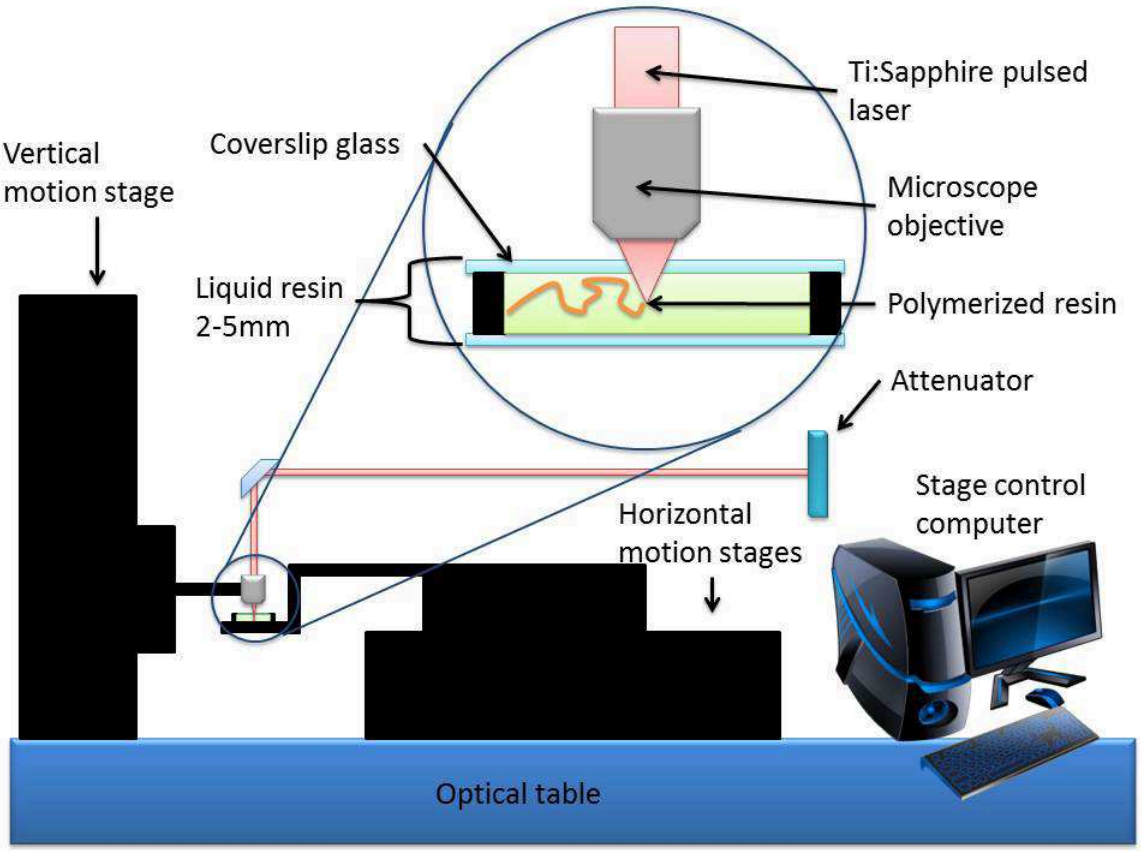

Figure 2.1: Experimental Setup

Experiments were carried out using both a commercial photoresist resin (SU-8) as well as resins formed by mixing commercially available monomers and photoinitiators. In this case, a resin was formulated using 90% triacrylate monomer (Sartomer SR-368) and 10% liquid photoinitiator (Esacure KTO-46) by weight. This resin therefore had 3.54×10^{26} photo-initiator molecules per cubic meter of resin. The composition will affect the resin sensitivity terms of the model. An amplified Ti:Sapphire 150 femto-second laser with an average output of 750 mW at $1,000$ Hz, and a Ti:Sapphire oscillator operating at 88 MHz with 320 mW average power were used. Each beam was first passed through an attenuator, and then through a focusing objective into the resin. The femto-second pulsed laser is used as this provides the high intensity necessary for two-photon polymerization.

$2-5$ mm of liquid resin was held between $0.15-0.2$ mm coverslip glass that was mounted on a tray attached to a computer-controlled X-Y horizontal motion stage, as seen in figure 2.1. The amount of liquid resin and thickness of the resin layer depends on the optical element used during the polymerization process and the size of the device being made. Since the devices are made without sacrificial bases and are net-shape, it is important to have a resin thickness larger than the overall device height. A g-code was used to trace out the part in the liquid resin.

The design used for the experiments is a block "M" sitting on four posts with a smaller "M" under the larger one, figure 2.2. This design was selected to demonstrate the ability of the two-photon polymerization process to create devices with sharp corners and undercut features in a single step.

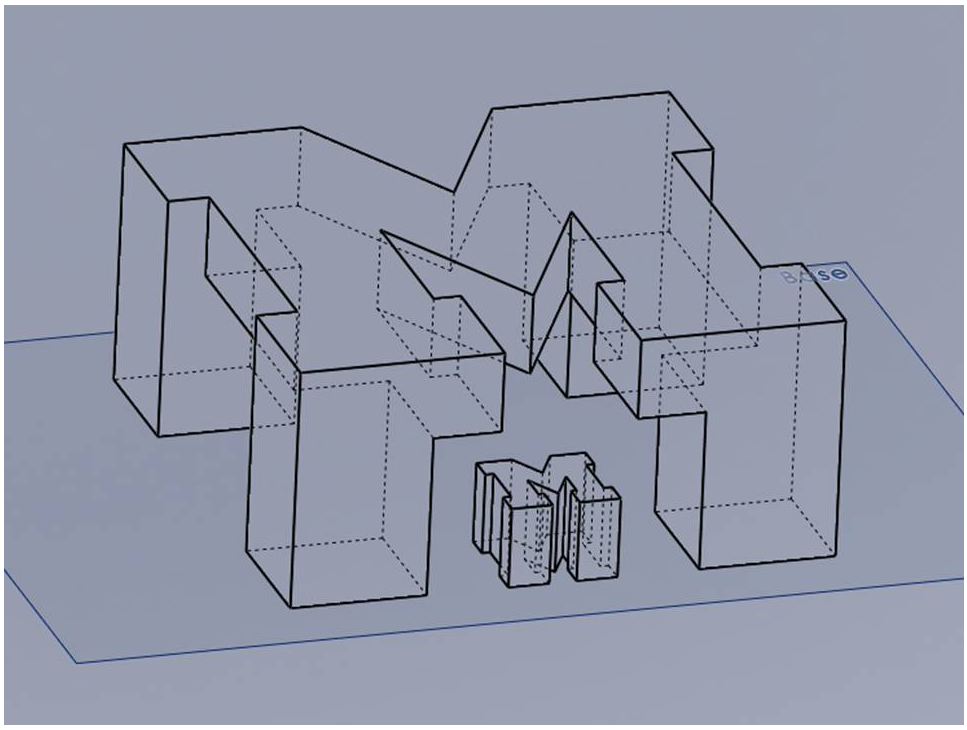

Figure 2.2: The design used for the experiments. The design is 250 μm in length and width.

The resin was polymerized using lenses with numerical apertures (NA) that ranged from 0.5 to 1.25, and power levels ranging from less than 1 mW to 50 mW. Other parameters that were varied in the experiment include the focal spot size as determined by the optical element used to focus the beam, and the speed of the motion stages, which varies the exposure time.

Once the devices were fabricated, the unpolymerized remaining liquid resin was washed from the solidified devices using methanol. Voxel diameters were measured by creating lines of polymerized resin. The devices were then imaged using an SEM, and from these images features of the devices were measured using ImageJ software package. Twelve measured data points were used in calculating an average voxel diameter.

2.4 Results and Discussion

SEM pictures of the parts created to demonstrate the process and also the voxel resolution are shown in figures 2.3(a) and 2.3(b). The resin used for these parts was the 10 % photoinitiator resin based on commercially available chemicals.

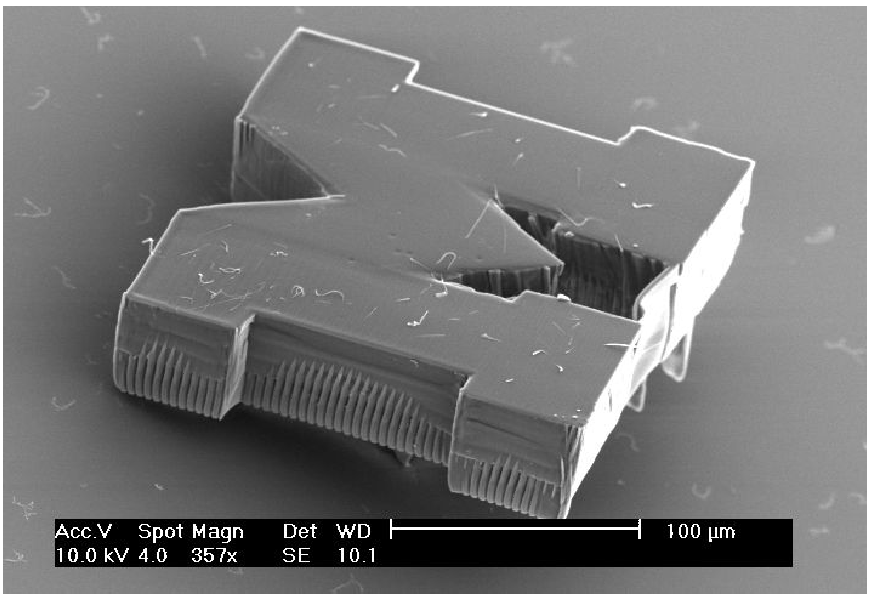

(a)

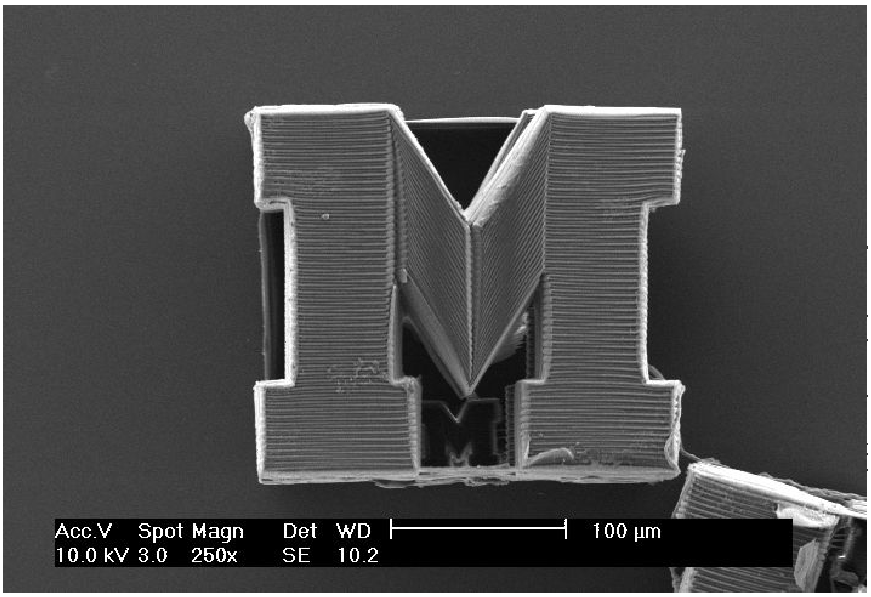

(b)

Figure 2.3: SEM of the M-block design (a) pictorial view, (b) top view

The thin strip connecting the two legs of the "M" fabricated in figure 2.4 were deliberately created to keep the legs in their respective positions, since the devices are formed without build support.

A sensitivity analysis was performed on the key model parameters, equation (2.16). A one percent change in each input parameter was modeled and the corresponding change in maximum voxel diameter calculated. The results are shown in Table 1. From Table 1, the voxel volume is found to be most sensitive to changes in the resin polymerization threshold, with the voxel volume decreasing as the polymerization threshold increases.

Table 1: Results of sensitivity analysis

	Voxel Diameter Change	
	without attenuation	with attenuation
Beam Diameter		
1 % increase	1.088 %	0.923 %
1 % decrease	-1.092 %	-0.929 %
Beam power		
1 % increase	1.455 %	1.340 %
1 % decrease	-1.451 %	-1.337 %
Resin threshold		
1 % increase	-1.437 %	-1.324 %
1 % decrease	1.470 %	1.354 %

The model developed, equation (2.16), shows that the amount of material that is polymerized increases with the square root of beam power. The corresponding experimental results are shown in figures 2.4 and 2.5. A polynomial model prediction curve of $VoxelDiameter \propto \sqrt{BeamPower}$ has been plotted for reference of the relationship between beam power and voxel diameter. With a circular voxel cross-section, the path width polymerized by the beam is equal to the voxel diameter. Error bars represent two standard deviations from the measured experimental data.

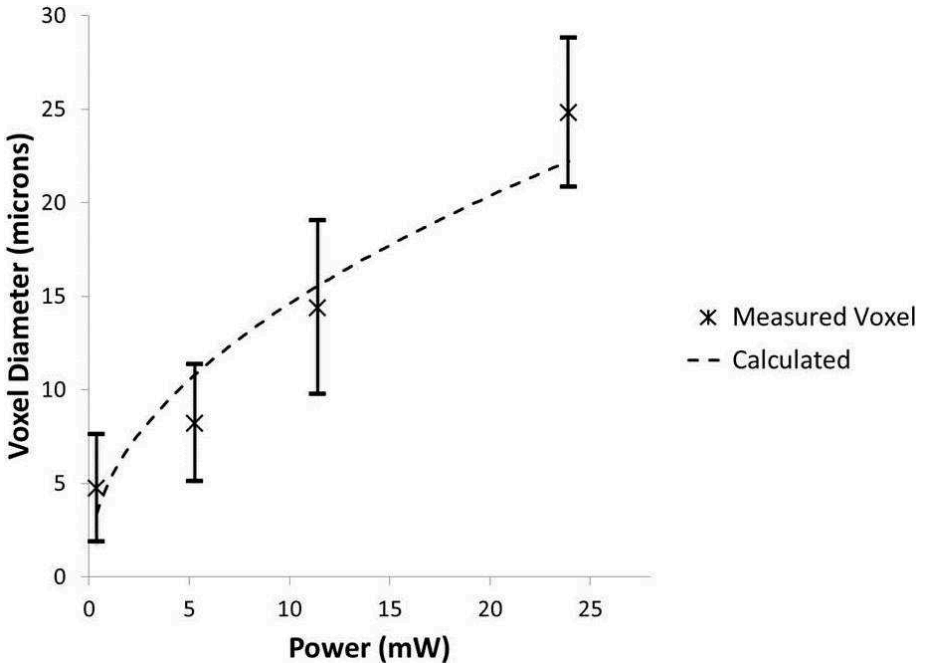

Figure 2.4: Variation of voxel diameter with input power, using 0.4 numerical aperture (NA) microscope objective. Error bars represent two standard deviations.

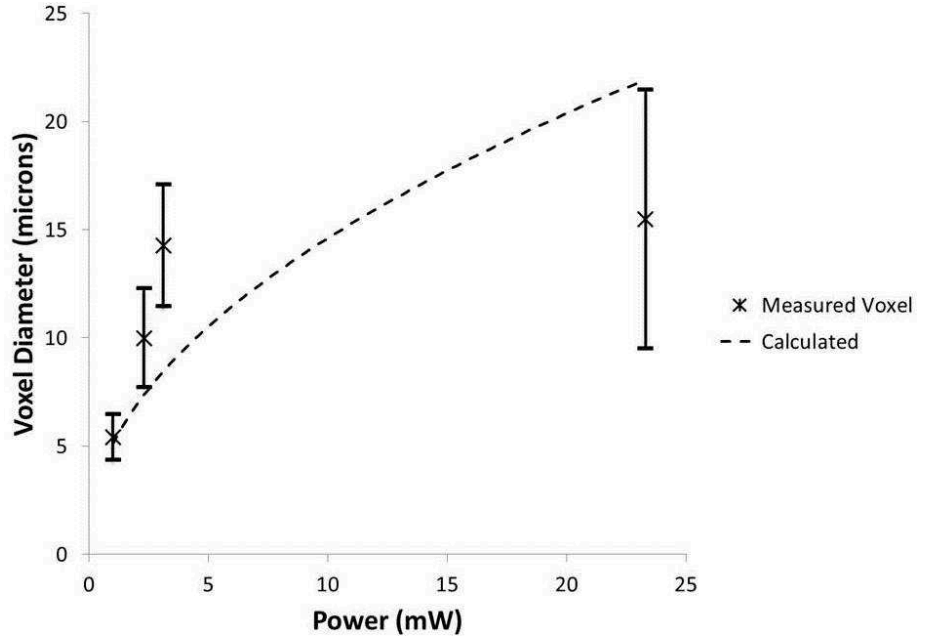

Figure 2.5: Variation of voxel diameter with input power, using 0.65 numerical aperture (NA) microscope objective. Error bars represent two standard deviations.

The voxel shape predicted by the model was also observed to become less spherical, figures 2.6 to 2.8, as the power increases. At higher power levels, polymerization extends beyond the beam diameter, figure 2.8, since the beam intensity is then high enough for polymerization outside the defined beam size, w. This leads to the shape seen in the model where the polymerization region is pinched near the focal point, following the shape of the focused beam, expanding outward away from the focal point as the beam does, until the intensity drops below the threshold needed for polymerization. In figures 2.6 to 2.8, the dashed line represents the beam envelope in the focal region, and the solid and composite lines represent the expected voxel size from the model. The solid voxel line takes into account attenuation of the beam power as it propagates through the resin. The composite voxel line (dashes and dots) represents the predicted voxel which does not account for beam attenuation. The ordinate represents the radial position (r direction), and the abscissa is the direction of beam propagation (z direction). At higher power, the voxel formed is no longer symmetric about the vertical axis, being larger on the leading side of the beam. The reduction in the voxel cross-sectional area is due to a reduction in the beam intensity as a result of absorption, as it propagates from right to left.

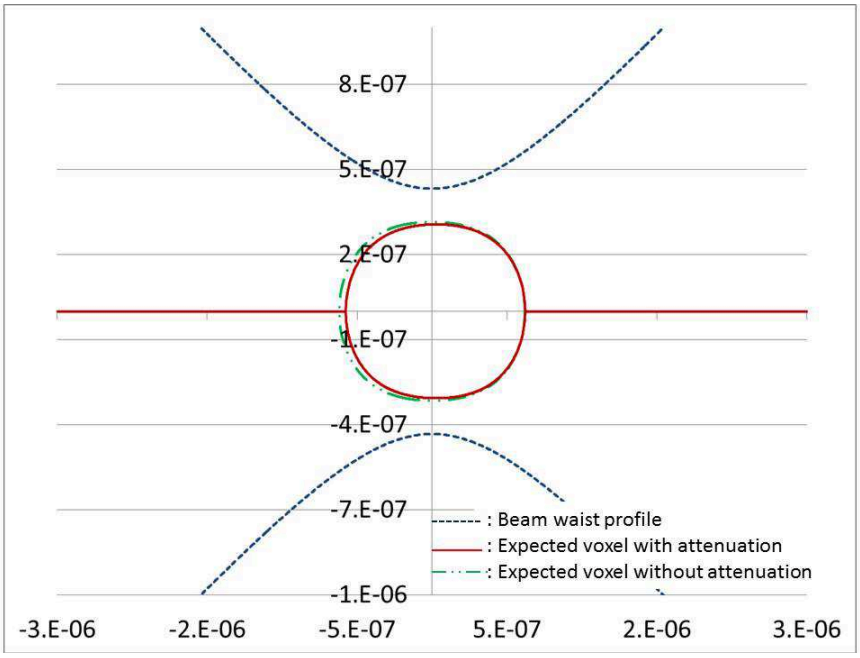

Figure 2.6: Voxel shape for low beam power with 0.65 NA focusing objective

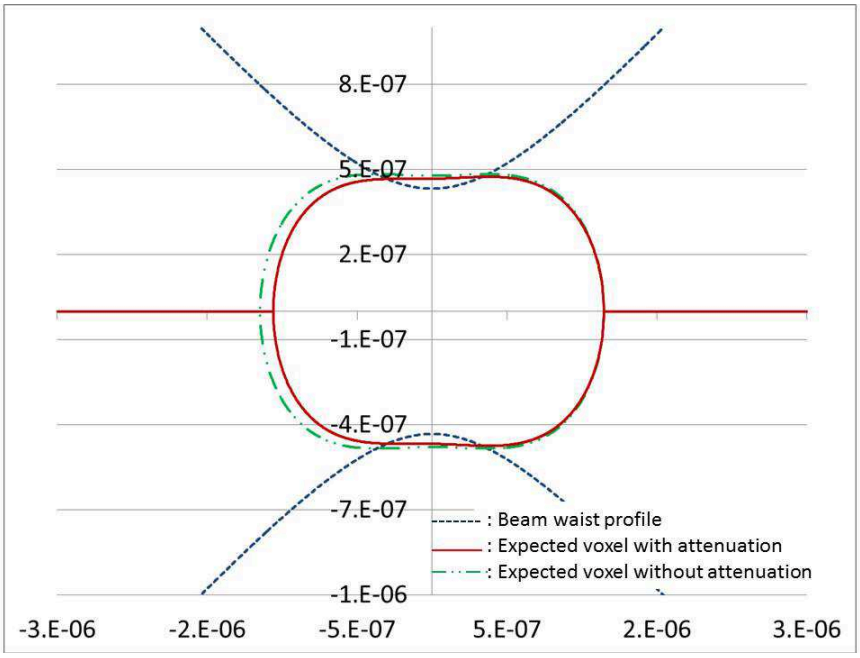

Figure 2.7: Voxel shape for intermediate beam power with 0.65 NA focusing objective

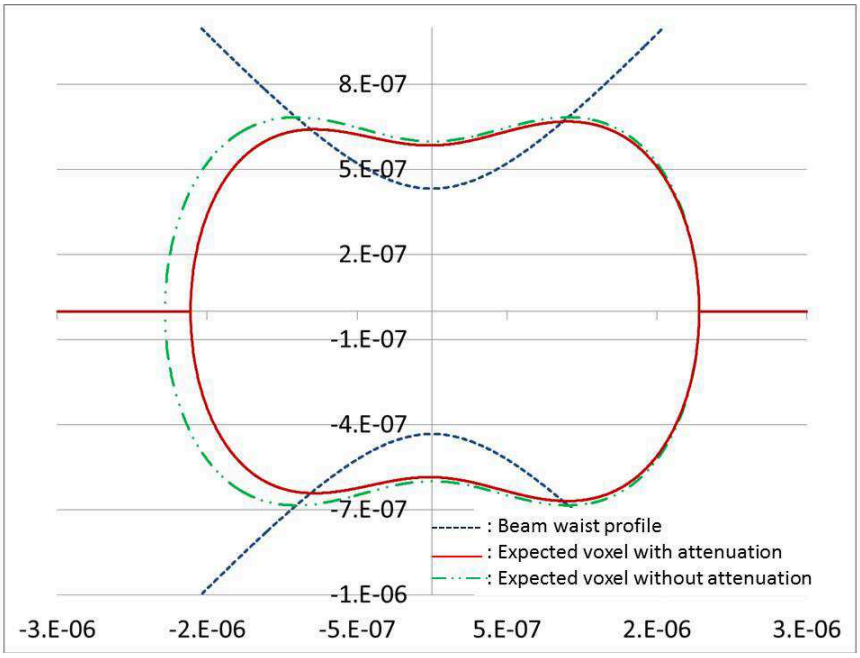

Figure 2.8: Voxel shape for high beam power with 0.65 NA focusing objective

The model, equation (2.16), also predicts a square root relationship between time and voxel size. Experimental results validate this relationship. As exposure time decreases, shown by increasing the traverse speed of the beam, the voxel size decreases, figure 2.9. Speed is shown in the plot instead of time as it is a controllable process parameter.

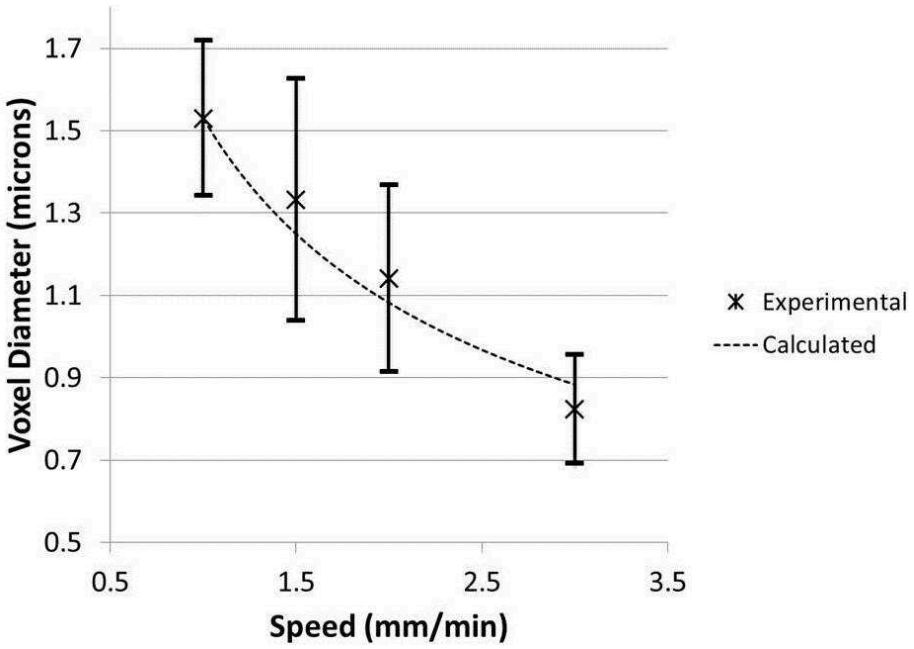

Figure 2.9: Variation of voxel size with traverse speed of the laser beam. Error bars represent two standard deviations.

2.5 Conclusions

A model for analytically determining the volume and shape of a voxel formed by two-photon polymerization has been developed. It takes into account the effects of several process parameters including beam power, lens numerical aperture (NA), resin sensitivity, and exposure time during the process. The analysis shows that the voxel volume is most sensitive to changes in the beam power at the focal point and the polymerization rate of the resin, and less sensitive to changes in beam diameter. It also shows that the voxel size increases with both the beam power and exposure time. Two-photon polymerization experiments demonstrated the validity of the model.

CHAPTER III

Methodology for Two-Photon Polymerization

Table of Variables

a_i	Set of points that describe the micro-device.
D	Total distance of laser path.
L_i	Length of ith section of laser path.
N	Number of points in a set a_i
P_j	Vector that connects points in laser path.

3.1 Introduction

The focus of this chapter is to provide an optimized procedure for creating a microdevice by two-photon polymerization. The process starts with a design of the device using a CAD package, which is used to generate the laser path, optimizing the laser path, and then controlling the laser-resin interaction during fabrication. The work presented optimizes the laser path for increased productivity, and elimination of unwanted features in the final device.

CAD and CAM programs that generate g-code to control motion stages are generally based on creating cutting tool paths resulting in the machining of a desired form. Two-photon polymerization, however, is similar to an additive process seen in other laser mi-

crofabrication processes, *Misawa and Juodkazis* (2006), where the desired solid form is traced by the focal point of the laser. Tool paths generated by traditional CAM programs are therefore not suitable for the two-photon polymerization process. The optimization of cutting tool paths in such works as *Sodemann and Mayor* (2008, 2011) is also not suitable to this application because of some of the unique processing capabilities when making microdevices by two-photon polymerization that differ from cutting processes. Developing a system for generating g-code from a CAD model and then optimizing the laser path taken is important because it will allow for faster production rates and higher resolution during the polymerization process as well as removing laser paths of undesired features in the part to be fabricated. In this chapter, an optimization routine is developed to generate g-code from a CAD model based on a modified greedy heuristic *Croitoru* (1982), *Sviridenko* (2000), *Lindberg et al.* (2010), following the traveling salesman problem (TSP) optimization method *Applegate et al.* (2009), *Kalantari et al.* (1985).

Two-photon polymerization has been shown to be a viable tool for micro-device fabrication *Kawata and Sun* (2003). Devices formed using this process include: miniature statues *Kawata et al.* (2001), micro-springs *Sun et al.* (2001a), micro-gears *Galajda and Ormos* (2001), micro-fluidic devices *Maruo and Inoue* (2006), as well as a method for creating wave guides *Davis et al.* (1996), and optical trap for manipulating micro-particles *Seibel* (2002). The micro-bull statue *Kawata et al.* (2001) which took three hours to fabricate, is shown in figure 3.1.

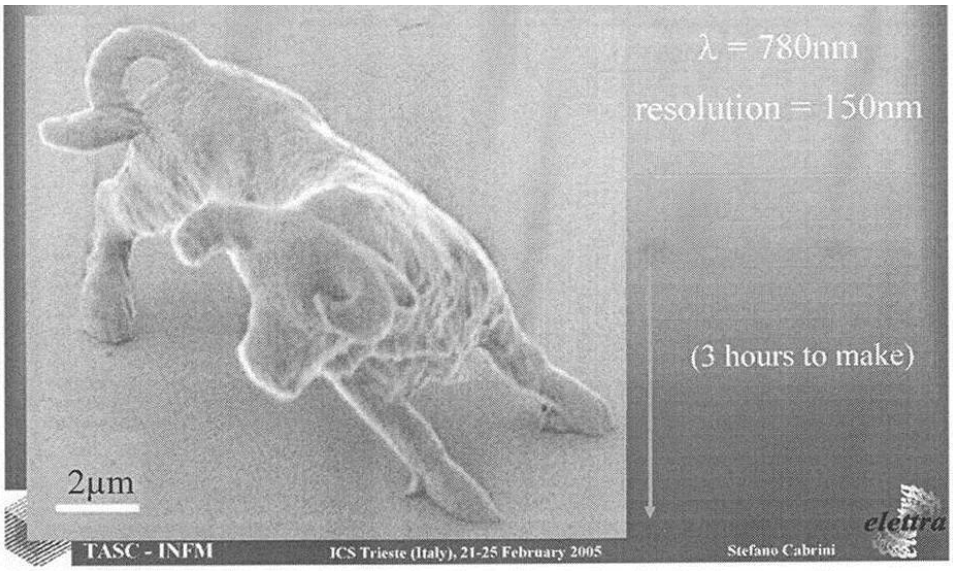

Figure 3.1: Photo of a micro-bull statue by *Kawata et al.* (2001)

This and other examples show the possibility for creating one-off micro-devices. The process of fabrication has been very slow and tedious, requiring several hours of fabrication time for devices of only a few cubic microns in size. The methodology presented in this chapter demonstrates the process for creating the micro-devices with an optimized laser path to minimize fabrication time as well as remove unwanted features.

3.2 Methodology for Creating Microdevices from CAD

To create the desired micro-device, a CAD design is first produced and a mesh is then applied to the surface of the device. The mesh creates a grid of points covering the surface of the device which will be the basis for generating the laser path as the part is fabricated. The set of points for the laser path is then optimized using the algorithm presented in this work to find the shortest path. This process optimizes production time and minimizes the scattered artifacts that occur from creating g-code directly from the mesh data. A g-code is then created from the mesh points to trace the part geometry.

The process of creating devices by two-photon polymerization can be summarized as follows:

1. Design the device using CAD
2. Apply a mesh to the surface that will describe the points where voxels are needed to form the device
3. Generate an initial laser path for the beam to follow to create the design
4. Optimize the laser path
5. Generate the g-code for the motion stages and beam attenuator
6. Run the fabrication with the selected focusing element
7. Post-process the device to remove the remaining liquid resin.

The major steps are further discussed in the following paragraphs.

In developing the CAD design, care must be taken to use the same units as those used for the motion stages. It is also beneficial to use a scale several times larger than the desired final device.

The CAD design is then opened in a 3D part management software package capable of applying a mesh. Applying the mesh on the surface of the design creates a set of points or vertices on the surface that defines the part. Figure 3.2 illustrates a device formed in a CAD package and with the mesh applied in the 3D part management software.

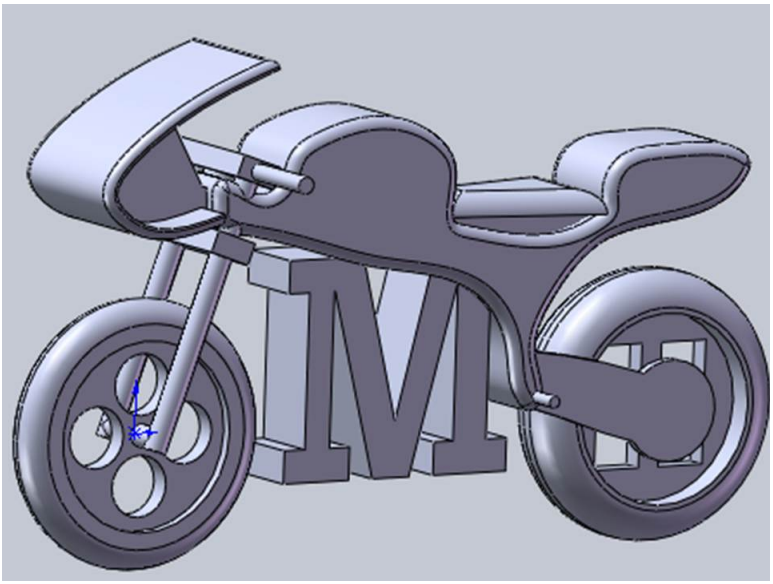

(a)

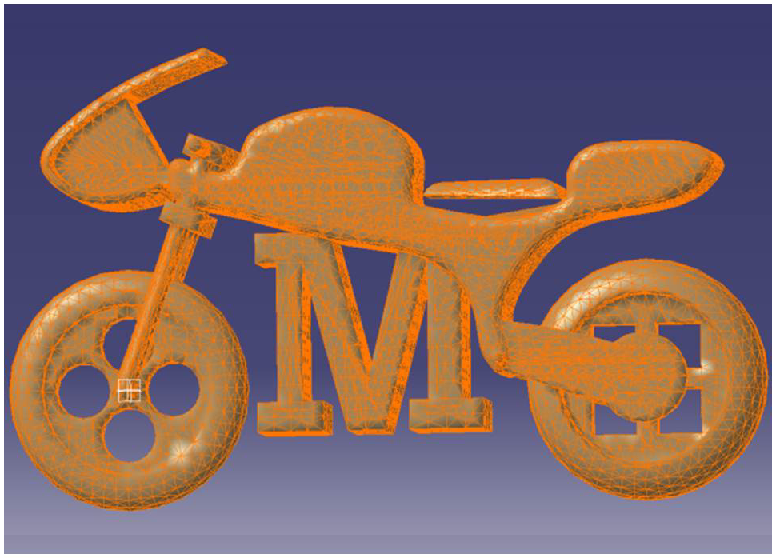

(b)

Figure 3.2: (a) CAD of the micro-bike design, (b) micro-bike with mesh applied

The set of points at the vertices of the mesh covering the part now defines the design to be used for creating the g-code. These are not necessarily ordered to produce the part with the shortest laser path.

In creating the part, the focal volume used for polymerization is moved through the resin by controlling the motion stages holding the resin as shown in figure 3.3. This allows

for arbitrary 3-dimensional devices to be created without the need for layering resin and processing it one step at a time.

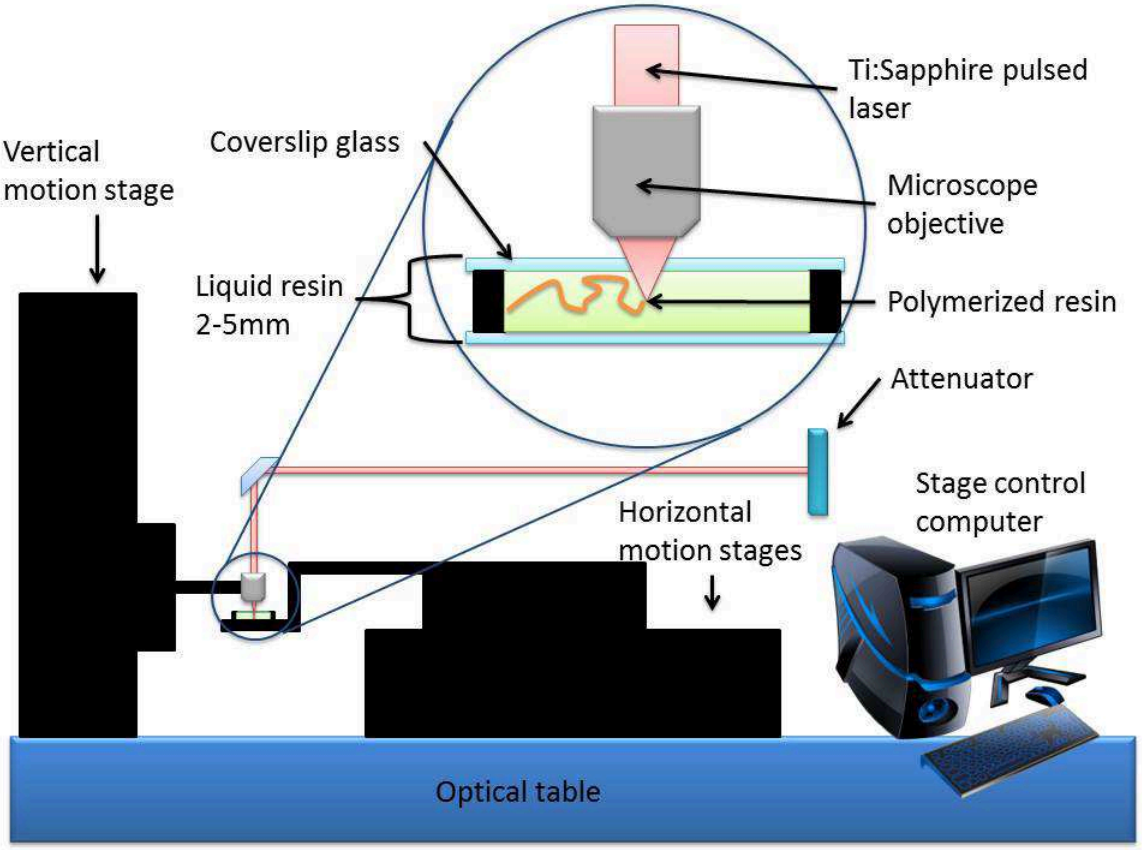

Figure 3.3: Experimental fabrication setup

The motion stages are controlled by the g-code which is created from the mesh point data by adding control sequences to the set of coordinate points that define the design. These control sequences vary the speed and power used to polymerize the resin.

Direct generation of the g-code from a mesh is not very efficient and leads to the laser path traveling in areas where solid features are not desired. This is because the points from the meshing process that are used to generate the g-code are not sequentially optimized for fabricating the device. This means the fabrication time will be greater than necessary and the laser will be traveling through paths that will generate undesired features. Optimizing the laser path reduces the processing time and eliminates unnecessary features, thus saving

cost and time. This work develops and demonstrates a methodology for optimizing the laser path for a single focal-point two-photon polymerization process.

3.3 Methodology for Laser Path Optimization

The optimization method developed in this work follows a traveling salesman problem where the laser must travel through all the points in the mesh to form the entire designed part. It is based on the greedy heuristic with the following assumption and initial condition: set the starting point for microdevice laser path optimization closest to the motion stage home location, and assume a single path can define the entire designed part. This assumption allows for a single calculation of an optimized laser path given the fixed starting point, rather than calculating the greedy heuristic optimization starting from every available point in the mesh. By selecting the starting point in the mesh and optimizing the laser path from this point, we can also fabricate multiple copies of the device by offsetting the home position within the same liquid resin sample after each device is made.

The g-code from CAD uses the Cartesian coordinate system. The process of optimization is done in principal planes ($X-Y$ plane for this application), and proceeds as follows: Initiate starting point; then find the next closest point by calculating the distance to all the neighboring points in the plane; continue finding the next nearest point until all points for the laser path have been completed. After all points in the $X-Y$ plane have been processed, the algorithm then moves on to the next Z level. This algorithm does not result in global path optimization, but rather a local optimized path in each Z plane.

The total path length taken by the laser to form the part can be defined as the sum of the lengths of paths that connect individual points in the mesh that defines the part. The cost function that must be minimized to produce the shortest laser path is:

$$D = \sum_{i=1}^{N} L_i \tag{3.1}$$

where each individual path segment between mesh points is:

$$L_i = \sqrt{(x_j - x_i)^2 + (y_j - y_i)^2 + (z_j - z_i)^2} \tag{3.2}$$

The objective is to find a point that would result in a non-zero length

$$(x_j, y_j, z_j) \in P_j \setminus \{a_i\} \tag{3.3}$$

that minimizes L_i, for the given set of points in the mesh:

$$a_i = \{(x_i, y_i, z_i) | i = 1, \ldots, N\} \tag{3.4}$$

and the set of available end points to connect to:

$$P_j = \{(x_j, y_j, z_j) | j = i, \ldots, N-1\} \tag{3.5}$$

This is subject to the constraint that the algorithm does not return to the last found point, and is achieved by removing the starting point from the set of possible points. As defined in the following expression, equation (3.6), the available points in the current set are equal to the points in the previous set excluding the current starting position:

$$P_j = P_{j-1} \setminus \{a_j\} \tag{3.6}$$

The following is a two dimensional illustration of the concept:

Define a_i as possible starting point in a given plane:

$$a_i = \{(x_i, y_i) | i = 1, \ldots, N\} \tag{3.7}$$

Let P_j be the remaining set of points in that plane:

$$P_j = \{(x_j, y_j) | j = i, \ldots, N-1\} \tag{3.8}$$

Starting at $i = 1$:

$a_1 = (x_1, y_1)$, find $(x_j, y_j) \in P_j \setminus \{a_1\}$ that minimizes L_i. Given that L_i for the 2-D case is:

$$L_i = \sqrt{(x_j - x_i)^2 + (y_j - y_i)^2} \tag{3.9}$$

and for $i = 1$, this becomes:

$$L_1 = \sqrt{(x_j - x_1)^2 + (y_j - y_1)^2} \tag{3.10}$$

Next, set $a_i = (x_j, y_j)$ for $i = 2$ which now represents the new starting point from which to find the shortest path length, then continue.

The data set for vector points P is then defined as:

$$P_2 = P_1 \setminus \{a_2\} \tag{3.11}$$

which is the set P_1 without points a_1 and a_2. This prevents the path from returning to the last point or resulting in a path of zero length. Minimizing the individual length vectors L_i, minimizes the overall cost function, thus resulting in the shortest laser path for fabricating the micro-device. Thus, the optimized laser path to follow is defined by the points in the ordered set, a_k:

$$a_k = \{(x_k, y_k) | k = 1, \ldots, N\} \tag{3.12}$$

This process of optimization was applied to the designed part in this work, by optimizing the laser path for each depth i.e., each Z-level. The algorithm is as follows:

1 initialize a ; initial starting point

2 do $z \leftarrow z + 1$; depth of $X - Y$-plane

3 do $i \leftarrow i+1$; for all mesh points in the $X-Y$ plane

4 compute distance for possible paths from i to all other points

5 compute the path from a to the next closest point, and store sequence of positions

6 eliminate the visited point

7 until visit all points in the $X-Y$-plane at given Z-level

8 return z

9 until total z is covered

10 end

To illustrate the concept, the design of the letter "M" was selected for simplicity. Figure 3.4 shows the paths generated directly from CAD, illustrating the additional lines that result from direct mesh generation. Using this as g-code will result in additional undesired features. In this example, only the perimeter of the "M" is to be polymerized.

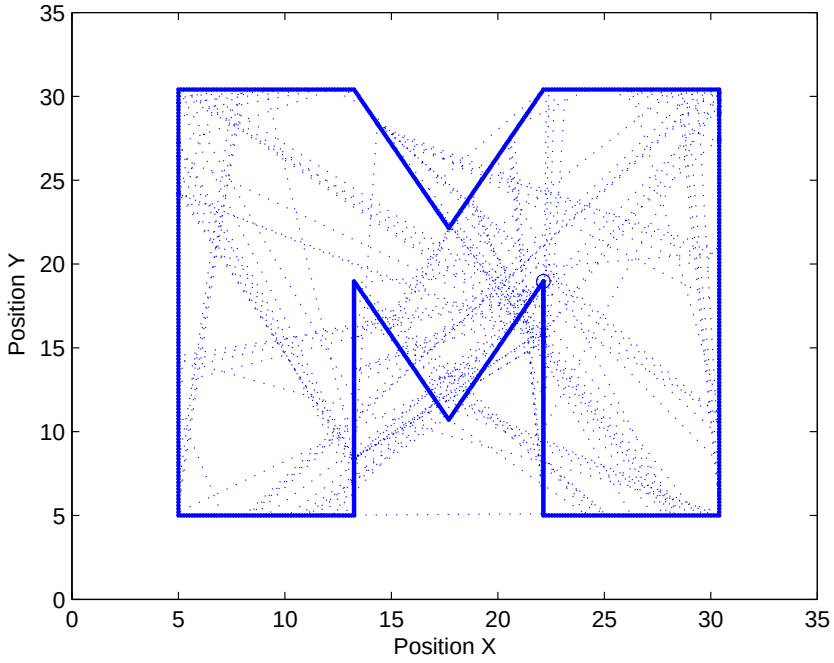

Figure 3.4: Example of laser path created directly from mesh data.

Application of the algorithm results in a final path that is shorter and clearer, figure 3.5.

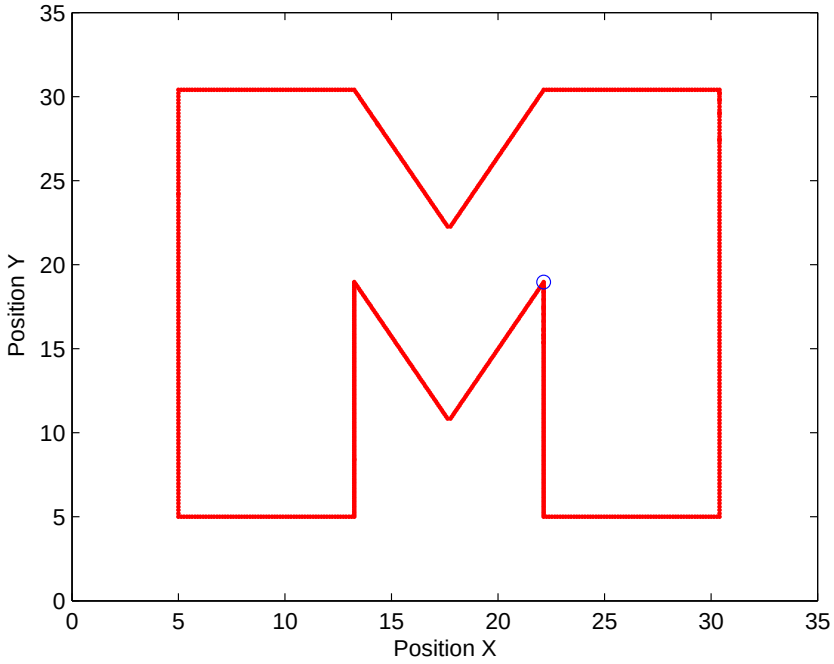

Figure 3.5: Example of optimized laser path.

3.3.1 Results of Sample Calculation

A sample micro-bike design, figure 3.2 was used to demonstrate the laser path optimization method. The following savings were calculated:

Total laser path distance from original g-code: 331mm

Total laser path distance with optimized g-code: 15mm

Laser path savings: 316mm

Optimized path is 22 times shorter.

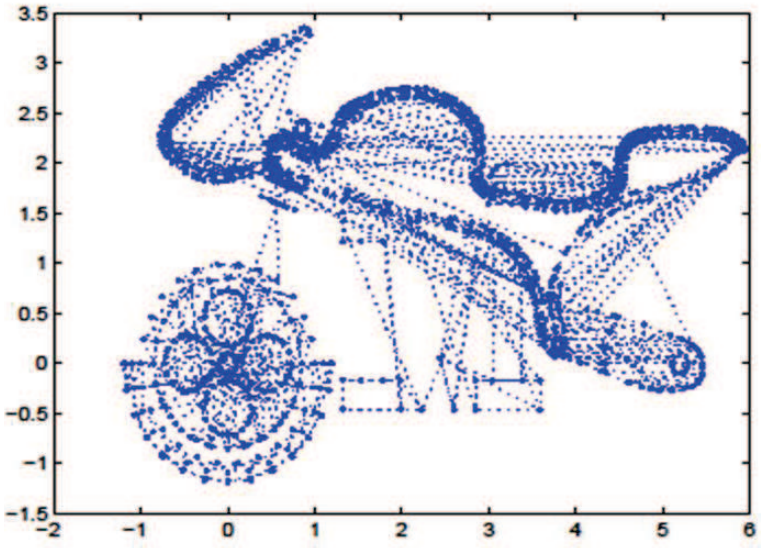

(a)

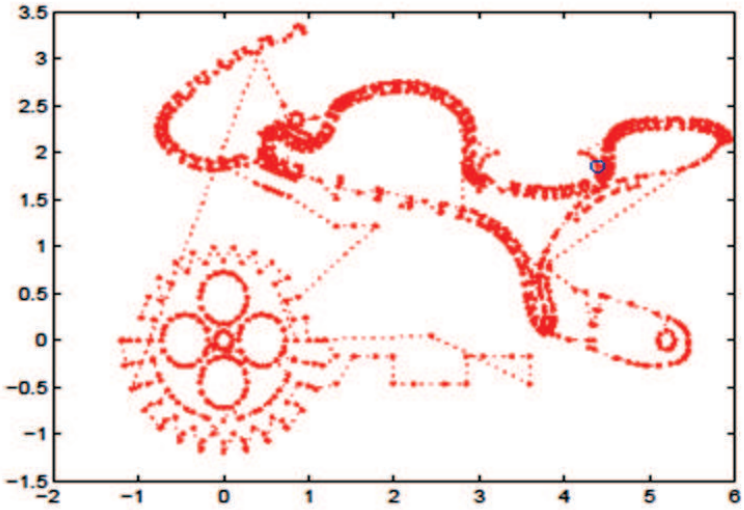

(b)

Figure 3.6: (a) Partial representation of laser path generated from original mesh data, (b) Part of optimized laser path

Figure 3.6(a) shows a cutaway of a single depth of the micro-bike laser path that was generated before any optimization was performed. Figure 3.6(b) shows the same cutaway after the laser path was optimized. Figure 3.7, shows an optical micrograph of the fabricated micro-bike.

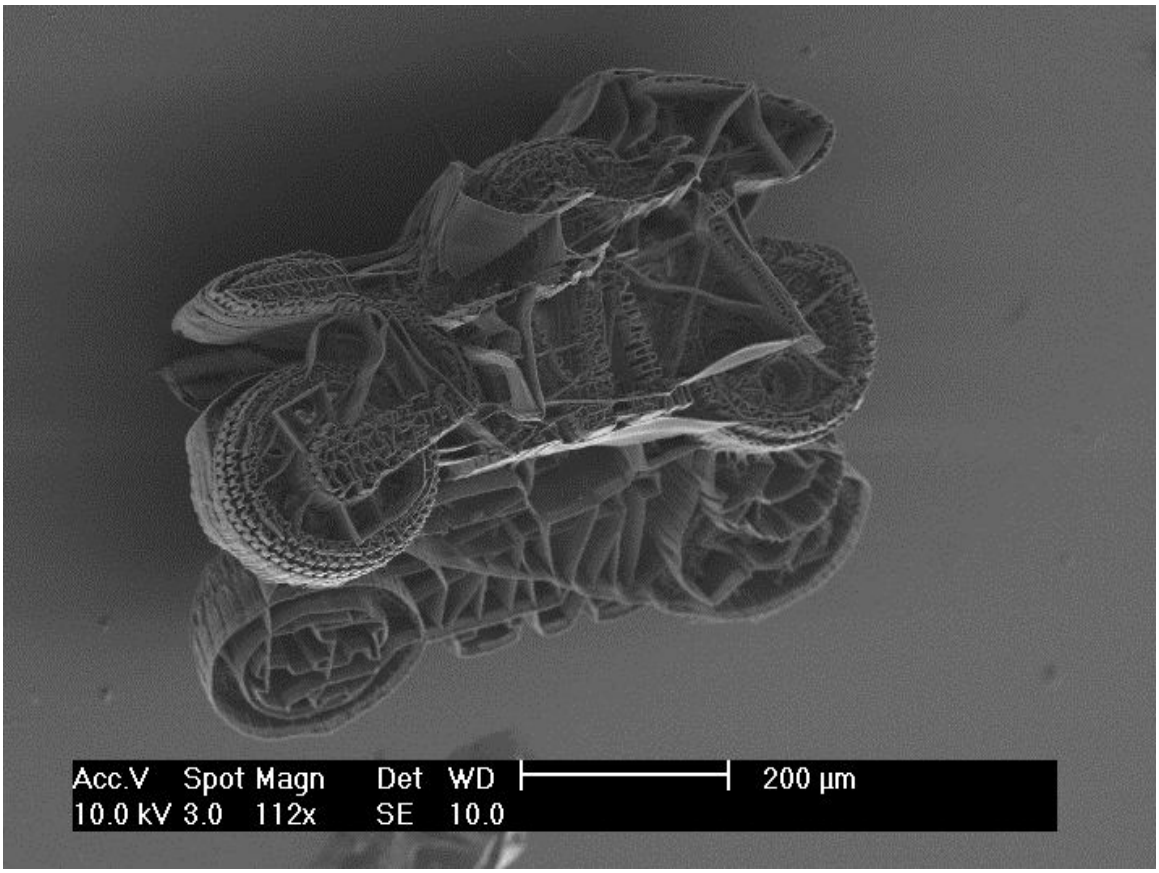

Figure 3.7: Micro-bike design fabricated with optimized path

As the results indicate, significant savings in processing cost can be achieved with the optimized laser path. For the example shown, the optimized path is 22 times shorter than the original mesh data. This enhances productivity and removes unwanted features from the end product.

3.4 Applying Process Parameters to Optimized g-code for Unwanted Feature Removal

Once the optimized laser path has been determined, the ordered set of points will enable the device to be fabricated using the shortest path. Doing so without controlling the power

will lead to the fabrication of unwanted features as the focal point jumps from one feature to another on the device. To prevent this, power and speed controls must be added to the g-code at these locations. For the fabrication setup used in this research, the power is controlled by an angular attenuator placed in the path of the beam. The speed of the motion stage can also be increased to accelerate the jump.

To determine the location of the jumps, the individual path length segments are calculated from the optimization section. Distances between two consecutive points that are several times greater than the mesh segment lengths set in the meshing operation are considered jumps. The power level at these jump segments are then attenuated to the lowest power setting to make sure no polymerization takes place during the jump, and the motion stage speed increased to minimize the time spent in that region.

Because of the pulsed nature of the beam, there will be an upper limit to the speed at which the beam can travel and still form a continuous solid object, especially for low repetition rate lasers. For a smooth structure, over of the laser pulses have to overlap.

3.5 Conclusions

In this chapter, a methodology is developed for creating micro-devices by two-photon polymerization, which optimizes the process for the laser path, using a modified greedy heuristic which is based on the traveling salesman problem. With this methodology it is possible to design and determine the process parameters for creating the micro-device by two-photon polymerization in an optimal fashion. It has also been shown that significant savings in processing time and removal of unwanted features can be achieved using the optimization algorithm developed. Following the presented methodology allows any three-dimensional micro-device within the operational limits of the manufacturing system to be created.

CHAPTER IV

Holographic Polymerization Model

Table of Variables

α	Phase difference of light from sources in the same slit. $\alpha = \frac{ka}{2}\sin\theta$.
β	Phase difference of light from same points in two slits. $\beta = \frac{kd}{2}\sin\theta$.
ϕ	Wave phase as a function of position z.
λ	Wavelength.
η	Hologram efficiency.
θ	Angle from normal plane of hologram.
a	Width of slits
A_0	Original reference wave amplitude.
$A(x,y,z)$	Reference wave equation.
A	Wave amplitude.
O_0	Original object wave amplitude.
$O(x,y,z)$	Object wave equation.
$R(x,y,z)$	Reconstruction wave.
d	Separation of slits.
k	Amplitude transmission coefficient.

I_k	Transmitted beam intensity.
I_0	Incident beam intensity.
I_θ	Intensity of the diffracted beam as a function of diffraction angle.
m	Integer for wave interference.
n	Integer for wave interference.
N	Number of slits.
t_0	Transmission coefficient.
T	Transmissivity.
t_p	Amplitude transmittance when hologram is reconstructed.
x, y, z	Cartesian coordinate system.

4.1 Introduction

In this chapter, holographic interferometry is analyzed as a potential tool for two-photon polymerization (TPP).

Two-photon polymerization is a process for manufacturing polymeric microdevices using the tightly focused energy from a femtosecond pulsed infrared laser. The process combines the two-photon absorption and free radical polymerization phenomena. Two-photon absorption is a special case of multiphoton effects which were first theorized in works by *Goeppert-Mayer* (1931), *Goeppert-Mayer and Born* (1931). During two-photon polymerization, energy from multiple photons excite photoinitiators thereby emitting free radicals, which then polymerize monomers that are susceptible to free radical polymerization. Since a very high intensity source is essential for the two-photon absorption effect, it only takes place at the focal point, solidifying a volume element, or voxel, at this location. Three dimensional microdevices can therefore be created in free form within the resin by tracing out the object features within the resin using the focal point. This contrasts with traditional lithographic rapid prototyping processes which require layer by layer processing.

The process of two-photon polymerization is achieved through free radical polymerization of the liquid resin by a photolytic process. The photons from the light source excite the photoinitiator molecules in the resin, creating free radicals which initiate the polymerization process. These free radicals join the monomers in the liquid resin to form chain radicals that grow in length by adding monomers to the chain. Polymerization is ended when chain radical molecules join to form a molecule with no radical activity.

Necessary conditions for TPP are:

1. Multiple photons arriving at the photo-initiator to excite the molecule.
2. Intensity of incident light on the photo-initiator must be adequate for polymerization.
3. Wavelength of the pulsed laser must be twice the excitation wavelength of the photoinitiator.
4. Resin must contain an adequate concentration of photo-initiator molecules.

In this chapter, the potential for using holograms for two-photon polymerization is investigated. A background on holograms is presented next.

4.1.1 Background on Holograms

A hologram is an optical element that uses the diffraction patterns of a coherent light source to create interference patterns of the light *Vest* (1979); *Saxby* (2004); *Hariharan* (2002); *Haines* (1966). These patterns can either interfere constructively or destructively.

Holograms allow for the creation of "bright, sharp, three-dimensional images" *Guenther* (1990), by recording the interference of a reference wave and signal wave. When the hologram is then illuminated with a reconstruction wave the interference patterns on the hologram create an image wave. This image wave is responsible for the creation of a real image and a virtual image. The virtual image formed can be seen with the human eye when

created, while the real image is a converging beam that recreates the original object used in creating the hologram. The real image formed by a conjugate of the original image used to form the hologram is of concern in this work as this is the portion of the created wave that converges.

A hologram is generally created using reference and object waves *Guenther* (1990). The object wave is described using the complex amplitude as:

$$O(x,y) = O_0(x,y)e^{-i\phi(x,y)} \tag{4.1}$$

And the reference wave complex amplitude is:

$$A(x,y) = A_0(x,y)e^{-i\Psi(x,y)} \tag{4.2}$$

where O_0 and A_0 are the original amplitudes, and $\phi(x,y)$ and $\psi(x,y)$ contain phase information.

Interference of the object and reference waves creates the interference pattern of the hologram:

$$I(x,y) = AA^* + OO^* + A^*O + AO^* = |A(x,y)|^2 + |O(x,y)|^2 + 2A_0O_0\cos\delta \tag{4.3}$$

where $\delta(x,y) = \Psi(x,y) - \phi(x,y)$ and A^* indicates the complex conjugate of A.

An example of a point object used to form a hologram and then illuminated to form the real object point is now presented to demonstrate the recreation of a focal spot size, figure 4.1. Starting with the planar reference wave having only z component *Guenther* (1990), the general form:

$$A(x,y,z) = A_0(x,y,z)e^{-i\psi(x,y,z)} \tag{4.4}$$

simplifies to:

$$A(z) = A_0 e^{-ikz} \tag{4.5}$$

The object wave being a point source can now be defined as:

$$O(x,y,z) = O_0(x,y,z)e^{-i\theta(x,y,z)} = O_0 e^{-ikr} \tag{4.6}$$

where

$$r = \sqrt{x^2 + y^2 + z^2} \tag{4.7}$$

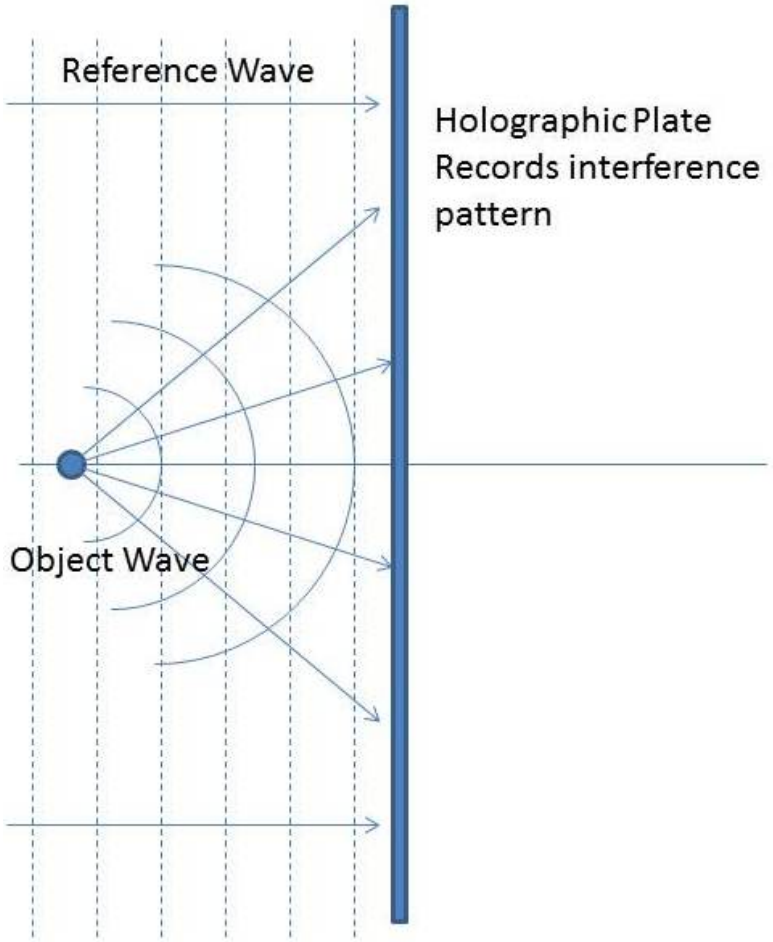

Figure 4.1: Creation of a hologram for a point.

The intensity distribution of the hologram, in terms of the object and reference waves, is then given as *Hariharan* (1996):

$$I(x,y) = |O+A|^2 = OO^\star + AA^\star + OA^\star + O^\star A \tag{4.8}$$

The resulting expression is real.

Transmittance through a hologram can now be defined as *Hariharan* (1996):

$$t = t_b + BEI(x,y) \tag{4.9}$$

where B is a parameter determined by the holographic material used, E is the exposure time, and t_b is background transmittance.

Substituting equation (4.8) into equation (4.9) results in *Hariharan* (1996):

$$t(x,y) = t_b + BE[|O+A|^2] = t_b + BE[OO^\star + AA^\star + OA^\star + O^\star A] \tag{4.10}$$

Reconstruction of the hologram is accomplished by illuminating with a coherent wave (which in this case is the same as the reference beam), resulting in the general form *Hariharan* (1996):

$$R(x,y) = C_r t(x,y) = \underbrace{C_r\left(t_b + BEA^2\right)}_{\text{direct wave}} + \underbrace{BEC_r|O(x,y)|^2}_{\text{negligible wave}} + \underbrace{BEA^2O(x,y)}_{\text{object wave}} + \underbrace{BEA^2O^\star(x,y)}_{\text{conjugate wave}} \tag{4.11}$$

which when written in terms of complex amplitudes becomes:

$$R(x,y)t_p = \underbrace{\left(t_b + B|A|^2\right)e^{ikz}}_{\text{direct wave}} + \underbrace{Be^{i2kz}e^{-ikr}}_{\text{conjugate wave}} + \underbrace{B|O|^2e^{ikr}}_{\text{object wave}} \tag{4.12}$$

where t_p represents the transmission through the hologram. The negligible wave term, which is much smaller than the other three terms in the reconstructed wave, is removed

because $|O(x,y)| \ll C_r$.

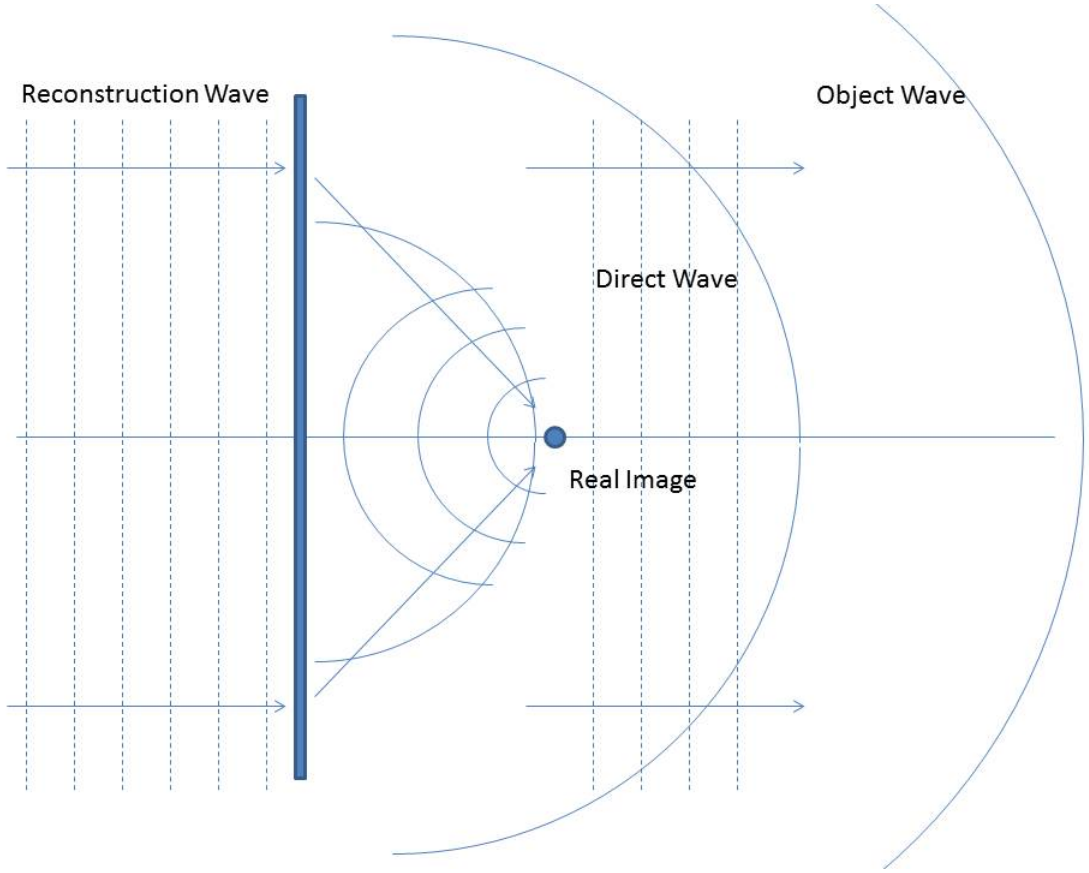

Figure 4.2: Reconstruction of a hologram

The direct wave is the same as the reconstruction wave with a change in amplitude. The conjugate wave term is a real image formed from the point source object. This portion of the reconstructed wave is what is considered for polymerizing the resin with some loss due to transmission efficiency. The object wave term is a wave creating a virtual image that can be seen by the eye.

A methodology for holographic polymerization is presented next.

4.2 Methodology for Holographic Polymerization

By analyzing the constructive and destructive interference patterns formed by a holographic diffraction grating, one can determine the regions where the light intensity will be

high enough for polymerization to occur. The regions of constructive interference depend on both the distance away from the hologram and the distance along an image plane.

The analysis, which is presented next, demonstrates the effect of constructive and destructive interference in varying the intensity at different positions defined by the real image of the hologram, and the potential for using holograms for polymerization. It is based on intensity relationships developed in the previous chapters, where regions within the resin where the intensity exceeds the minimum threshold for exciting the photoinitiator molecules is where polymerization is considered to take place.

4.2.1 Model for Holographic Polymerization

Diffraction gratings are used as a starting point to create a model of the intensity distribution at every position of the waves formed by the hologram. This principle of constructive and destructive interference from diffracted light sources will form the basis for determining the locations of polymerization expected when using holographic optical elements in two-photon polymerization. This holographic model for polymerization formulation begins with the analysis of a two slit model *Guenther* (1990) to explain the effects of light diffracting and interfering from multiple sources, as takes place when a hologram is illuminated to create the real image.

$$I_\theta = \left(\frac{\sin^2 \alpha}{\alpha^2} \cos^2 \beta \right) \tag{4.13}$$

where I_θ is the intensity distribution as a function of angular position θ, α is the phase difference of light from sources in the same slit ($\alpha = \frac{ka}{2} \sin\theta$), β is the phase difference of light from same points in two slits ($\beta = \frac{kd}{2} \sin\theta$), and a and d are the slit width and separation, respectively.

The location and intensities of the regions of constructive interference are determined using Bragg's law *Guenther* (1990):

$$2d\sin\theta = n\lambda \tag{4.14}$$

where $d =$ distance between slits (or fringes for a hologram), θ is the angle from normal plane of hologram, n is an integer, and λ is the wavelength of light.

The principal maxima of the interference pattern are given by:

$$I_{\theta P} = N^2 I_0 \frac{\sin^2\alpha}{\alpha} \tag{4.15}$$

where $\alpha = \frac{ka}{2}\sin\theta_x$, propagation constant $k = \frac{w}{c} = \frac{2\pi}{\lambda}$, and N is the number of slits.

The secondary maxima are given by:

$$I_{\theta S} \approx I_0 \frac{\sin^2\alpha}{\alpha}\left[\frac{2N}{\pi(2m+1)}\right]^2 \tag{4.16}$$

The ratio of intensities of the principal and secondary maxima is then given by:

$$\frac{I_{\theta S}}{I_{\theta P}} = \left[\frac{2}{\pi(2m+1)}\right]^2 \tag{4.17}$$

$$\beta = \frac{m}{N}\pi = \frac{kd}{2}\sin\theta_x \tag{4.18}$$

Figure 4.3 shows the intensity profile from a 2-slit diffraction grating. The vertical axis represents the intensity in arbitrary units, while the horizontal axis represents the distance along the plane in which the beams are interfering. This is a one dimensional case.

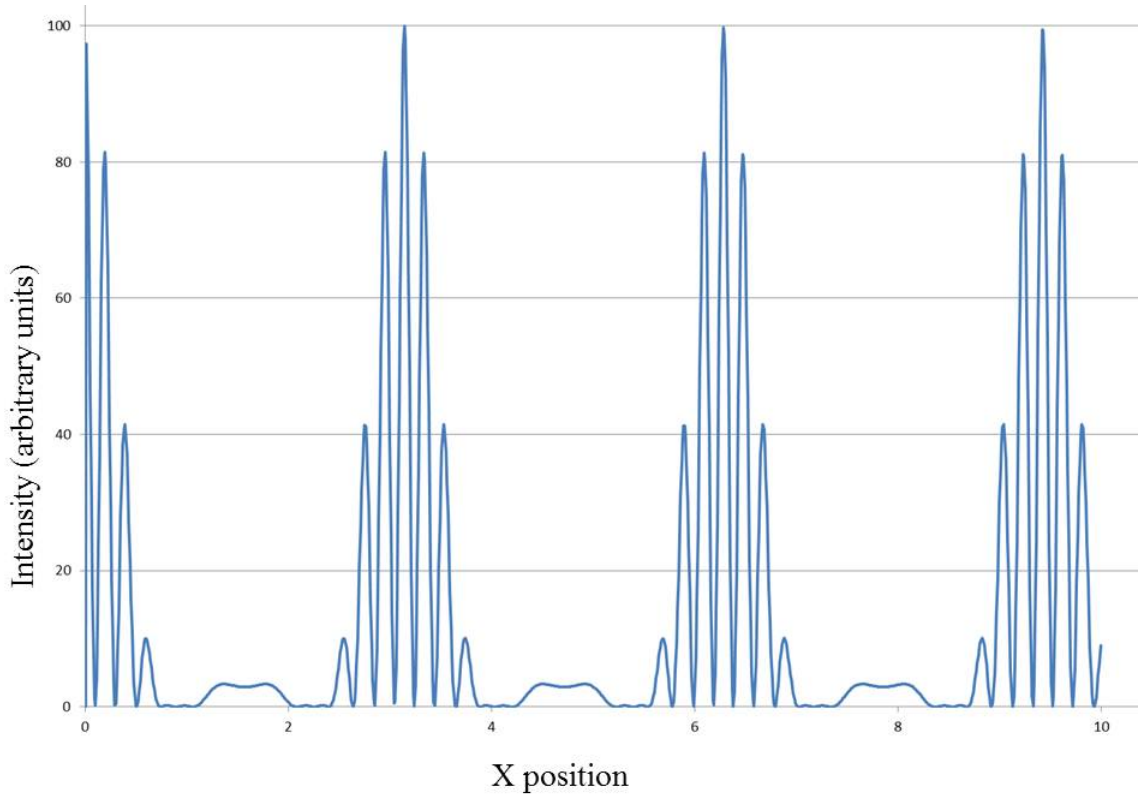

Figure 4.3: Interference pattern of a two-slit model

Building on the two-slit model *Guenther* (1990), the wave interference can be expanded to N-slits of repeating rectangles by applying the two-slit interference method from equation (4.13) to the orthogonal directions x and y:

$$I_{\theta(x,y)} = \left(\frac{\sin^2 \alpha_x}{\alpha_x^2}\frac{\sin^2 N_x\beta_x}{\sin^2 \beta_x}\right)\left(\frac{\sin^2 \alpha_y}{\alpha_y^2}\frac{\sin^2 N_y\beta_y}{\sin^2 \beta_y}\right) \tag{4.19}$$

Figure 4.4 represents the slit height and width as well as the spacing between slits used for modeling the system. This figure represents the basic diffraction grating used to calculate the interference patterns.

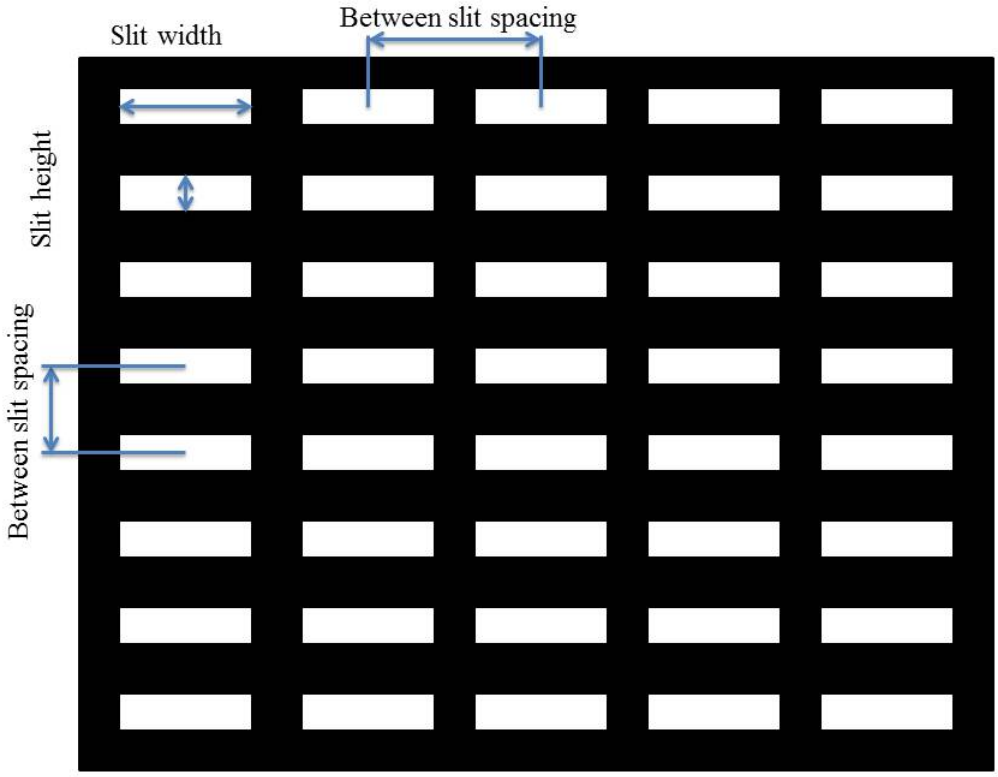

Figure 4.4: Hologram of rectangular slits

Figures 4.5 through 4.8 represent the intensity profiles of N-slits of repeating rectangles. The surface height represents the intensity in arbitrary units at every position in the plane.

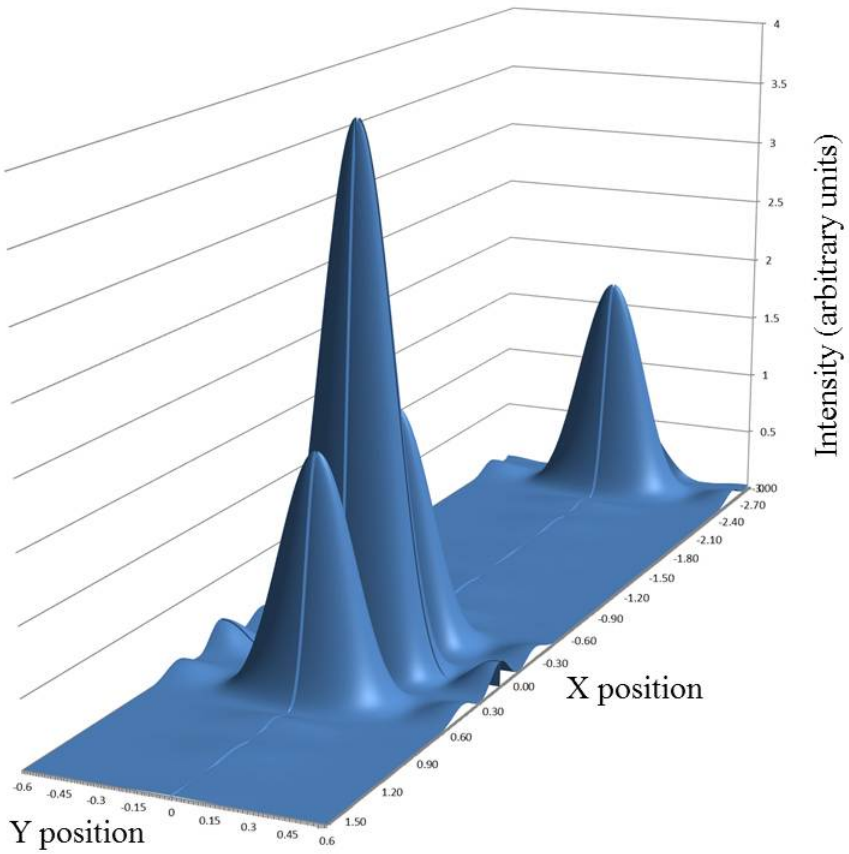

Figure 4.5: Holographic diffraction grating. *x* direction: 2 slits with spacing of 2 times the slit width. *y* direction: 1 slit.

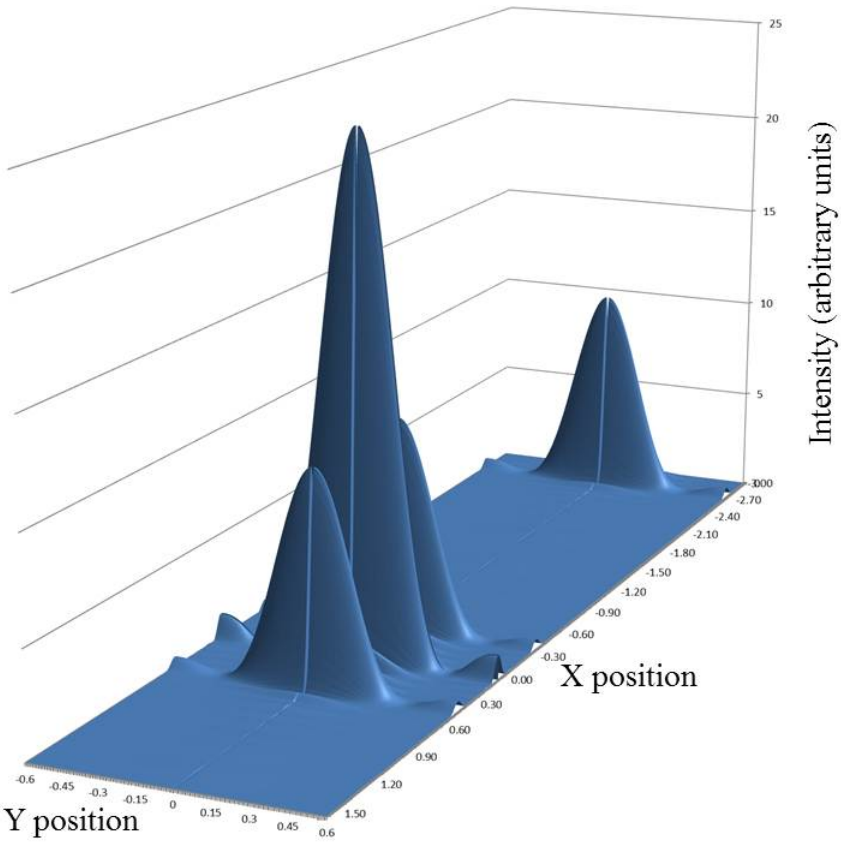

Figure 4.6: Holographic diffraction grating. x direction: 5 slits with spacing of 2 times the slit width. y direction: 1 slit.

As the number of slits along an axis increases, the locations of constructive interference become more narrowly defined. The spread of the intensity peak is much more narrow, figures 4.5 and 4.6. When the slit spacing is increased the locations of constructive interference increase, figures 4.7 and 4.8.

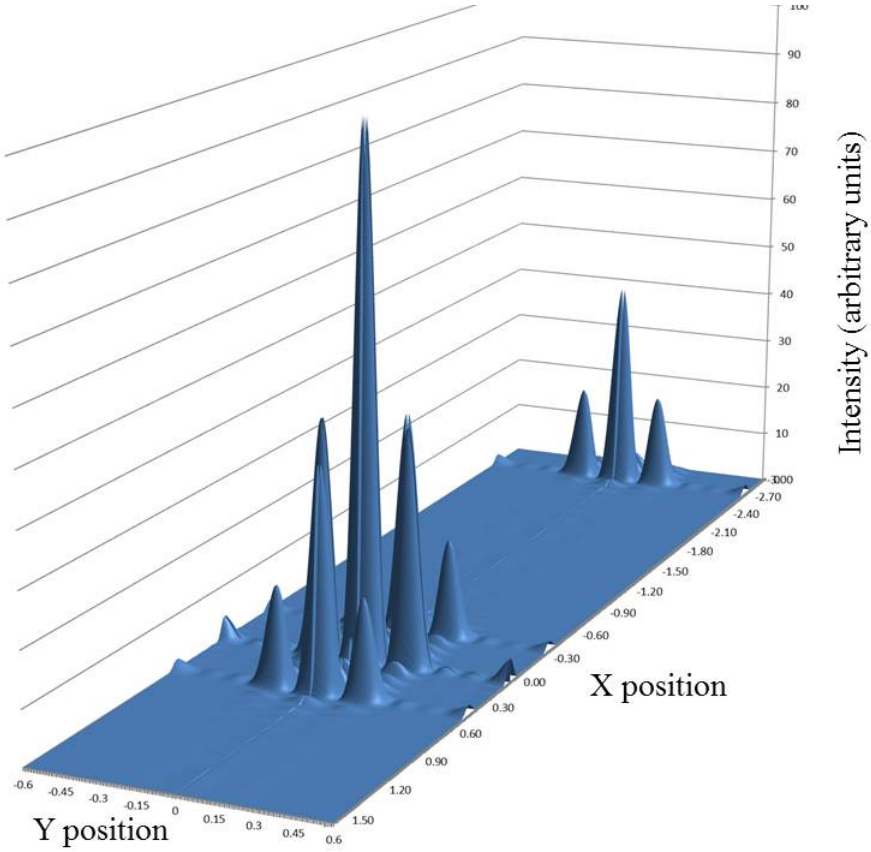

Figure 4.7: Holographic diffraction grating. *x* direction: 5 slits with spacing of 2 times the slit width. *y* direction: 2 slits with spacing of 2 times the slit width.

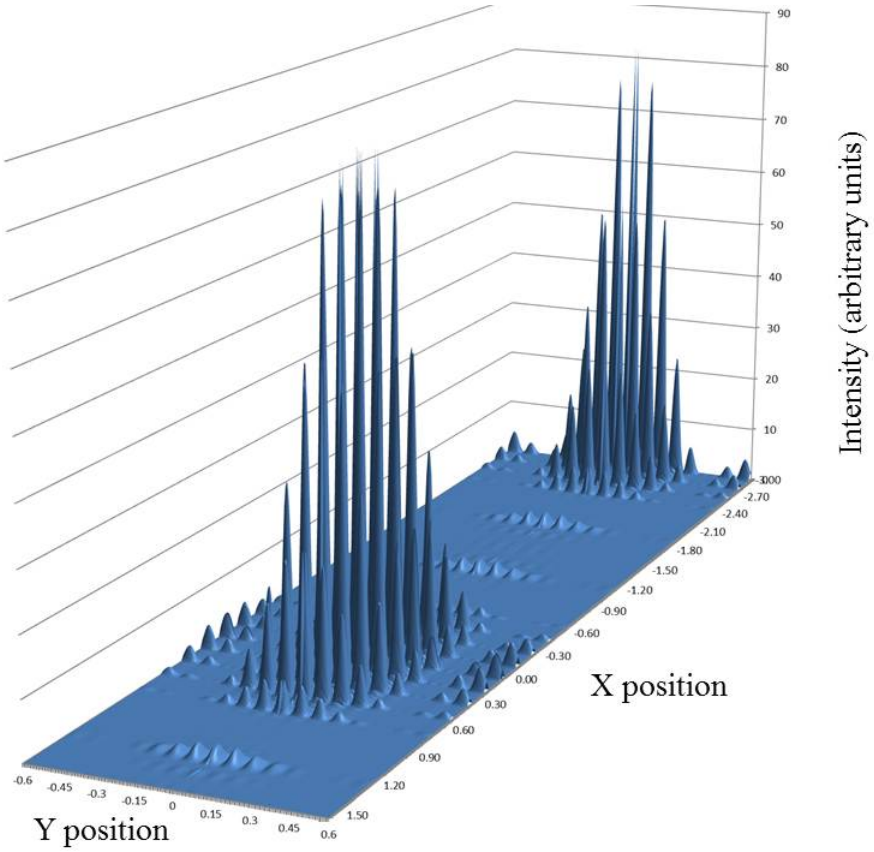

Figure 4.8: Holographic diffraction grating. x direction: 5 slits with spacing of 5 times the slit width. y direction: 2 slits with spacing of 5 times the slit width.

The intensity of a beam that is passed through a hologram can be expressed as:

$$I_k = I_0 k^2 = I_0 T \tag{4.20}$$

where I_k is the transmitted intensity, I_0 is the reconstruction intensity, k is the amplitude transmission coefficient, and T is the transmissivity.

4.3 Application to Two-Photon Polymerization

From previous chapters it has been shown that the two-photon polymerization process has an intensity based relationship. From this basis the intensity profile formed by the

hologram will be applied to the polymerization model to determine the regions of expected polymerization.

The holographic diffraction grating analysis in the preceding paragraphs can be expanded to constructive and destructive interference of arbitrary holograms. The real image of holograms are locations where rays from holograms constructively interfere, and with adequate intensity, polymerization can take place.

Other work has shown that computers can be used to generate holograms *Marsh and Smith* (1976), and that higher order terms of the hologram can be removed by adding interference patterns to the computer generated hologram, so that only the real image and reconstruction waves remain *Pavillon et al.* (2010); *Ma et al.* (2012). Work has also been done on the design of holographic optical elements and the efficiency of these tools *Awatsuji et al.* (2002). Thus it should be possible to use computer enhanced holography to enable only the desired shape to be produced by two-photon polymerization.

4.3.1 Model Application to Laser-Resin Interaction

As with single focal point polymerization using a singlet lens or compound microscope objective the laser-resin interaction for two-photon polymerization requires that the photons arrive at the location of interest within a short time period of each other, and with an intensity that exceeds the minimum intensity threshold for polymerization. In this case the hologram replaces the lenses and serves as the optical element for creating regions of varying intensities to determine locations for polymerization. Methods for tracing rays through holograms have been presented by others *Olson* (1989). Combining the holographic theory presented in the preceding sections with the single focal point model from previous chapters will enable the regions where the intensity will be adequate for polymerization to be mapped. These will be those locations where the transmitted hologram light intensity is greater than or equal to the minimum threshold intensity for polymerization, $I_h \geq I_{thres}$. Using a diffraction grating as described in the earlier model formulation would allow for

the creation of simple repeating patterns within the liquid resin using a single holographic optical element, where others have shown the use of lasers in ablating material by interfering multiple beams *Nakata et al.* (2004) to creating repeating structures, using holographic optical elements in two-photon polymerization would polymerize targeted regions.

The methodology presented here provides a novel approach to TPP through the use of holographic optical elements. This will enable computer generated holograms to be incorporated into the fabrication of large surfaces of microdevices by exposing large areas to intensities that exceed the threshold intensity for polymerization.

This methodology has the benefit of increased production methods due to the exposure of large areas using a single hologram.

4.4 Conclusions

Holography is investigated as a potential tool for enhancing productivity of the two-photon polymerization process. It is shown that holographic optical elements represent a viable tool for creating complex devices by two-photon polymerization. The intensity distribution of the image in a three-dimensional space that results from constructive interference will enable the resin to be polymerized as such locations as to create an object that corresponds to the image.

The significance of this work is the potential for large scale application of the two-photon polymerization methodology.

Novel contributions from this work stem from the development of the model which demonstrates the feasibility and methodology for using holographic optical elements in two-photon polymerization.

CHAPTER V

Hardware for Two-Photon Polymerization

5.1 Introduction

The focus of this chapter is to provide details on the hardware implementation developed for the reconfigurable manufacturing system for micro-device fabrication using two-photon polymerization. In the previous chapters the process for two-photon polymerization was presented and the methodology for creating an object from CAD to the machine control code (g-code) was presented. Current research in the fabrication of micro-devices by two-photon polymerization use hardware and software that are limited to use in the lab for creating prototype micro-devices. This current method means that the fabrication hardware is built around the laser system used and designed with a fixed optical element for focusing the beam. This type of system limits the size and applications of the microdevices made by two-photon polymerization. This chapter describes the work done to develop a reconfigurable manufacturing system for two-photon polymerization (RMS-TPP) that can work with a variety of laser systems and can be reconfigured to use a variety of optical elements depending on the manufacturing specifications of the micro-devices being made.

This reconfigurable manufacturing system for two-photon polymerization (RMS-TPP) design allows it to be used as a closed box solution to fabricate micro-devices.

The concept for this RMS-TPP production system is based on reconfigurability which allows the system to work with a variety of femto-second laser systems and optical focusing

elements based on the feature resolution and size of the final micro-device being made. Also important to the design and development of this system is the compatibility with current computer numerical controlled manufacturing tools found on the manufacturing floor.

This chapter describes the design of the RMS-TPP.

5.2 Prototype Manufacturing System Design Specification

The RMS-TPP needs high accuracy, precision, common code used on manufacturing floor, repeatability, and reconfigurability.

For the reason a system based on cutting edge medical device manufacturing was used as a base platform.

The building blocks of the RMS-TPP are divided into mechanical components, control hardware, and the electrical and computer software.

The mechanical components consist of:

- Orthogonal linear motion stages for (X-Y) motion.
- Vertical linear motion stage for (Z) motion.
- Linear motion stages with a resolution of 0.005 μm for each axis, and the vertical position was controlled by moving the focusing element, also with a 0.005 μm resolution along the z-axis.
- Rotational motion stage: attenuator mounted to allow for computer control of the beam power incident on the lens.
- Lenses: mounted to the vertical motion stage, and allowing for reconfigurability without having to realign the laser beam.
- Attenuator: crystal mounted to rotational motion stage, that is compatible with wide range of power levels to work with both oscillator only and amplified femto-second pulsed laser systems.
- Mirrors: high reflectivity for IR beam.

- Telescope: expands incoming beam to cover the optical focusing element.

Details of how components are connected can be seen in figures 5.1 and 5.2.

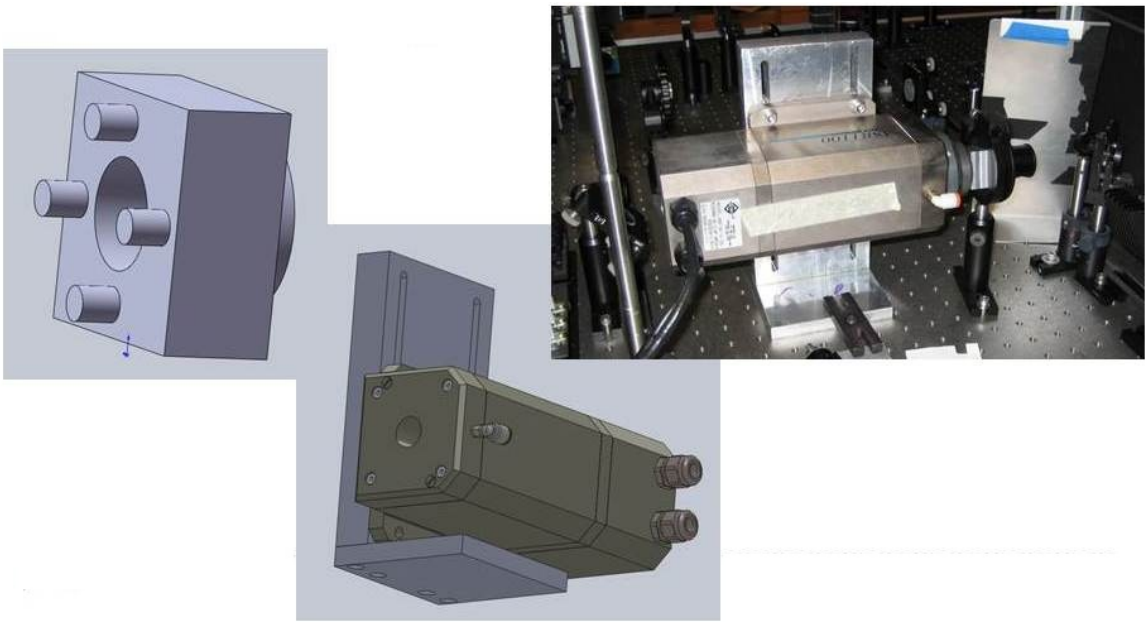

Figure 5.1: Hardware for prototype manufacturing system

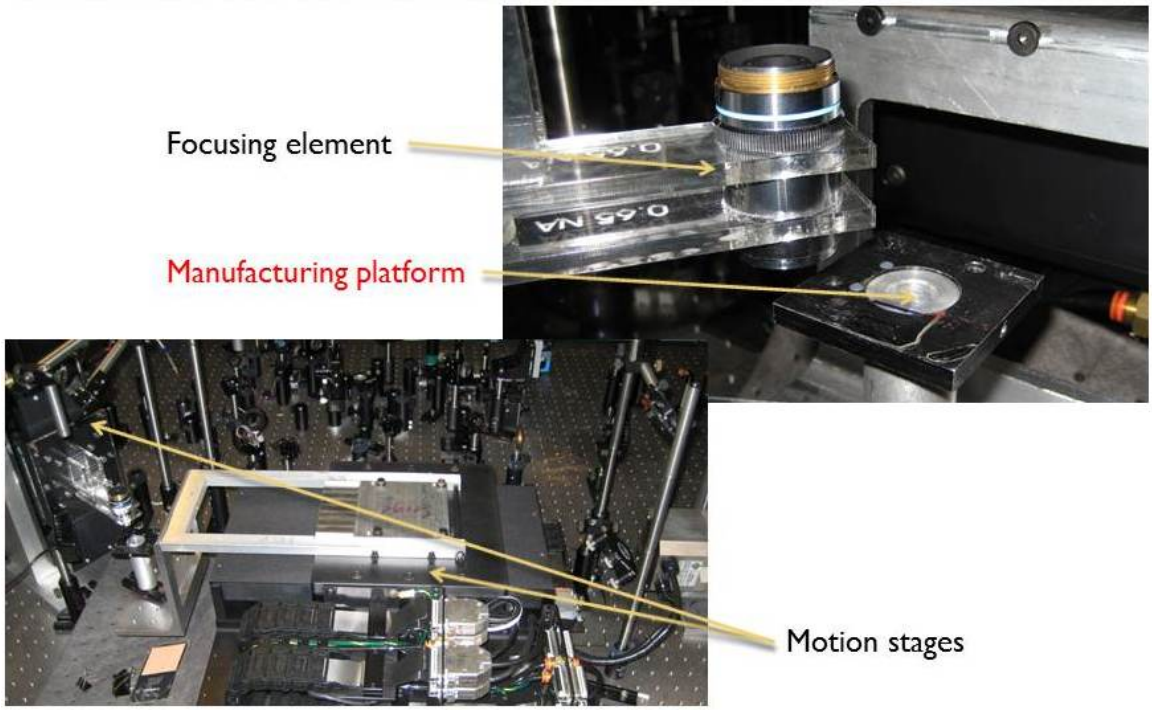

Figure 5.2: Manufacturing System Details

Reconfigurability of this manufacturing system is enabled by switching the optical focusing element based on product family. These optical elements share a common mounting architecture to allow the system to be reconfigured without having to realign the laser beam. The telescope can also be reconfigured to allow for a range of laser beam diameters. The mirrors at the input of the manufacturing system are mounted to align beam into manufacturing system, and adapt to a range of incoming beam paths.

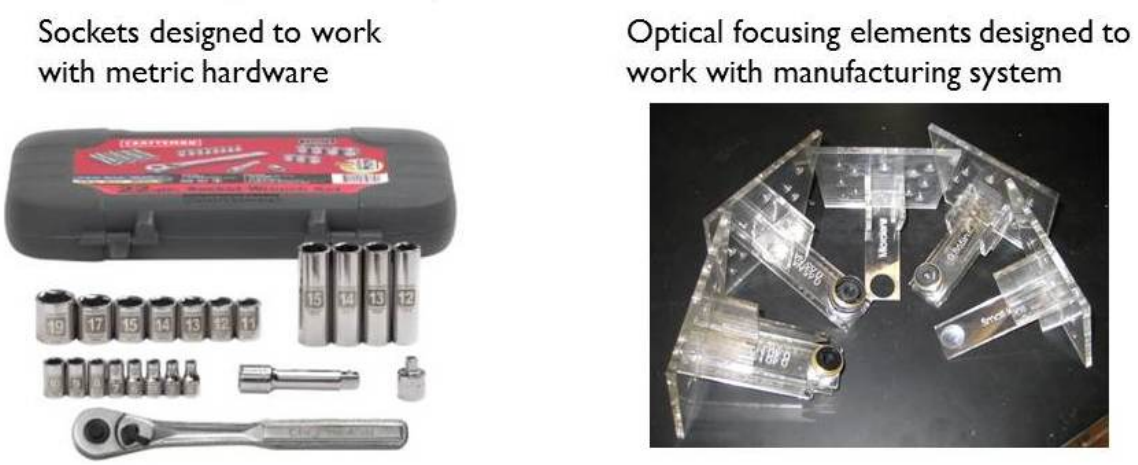

Figure 5.3: Reconfigurability of RMS-TPP

Hardware and software connections: hardware has a common connector for all stages, linear and rotational. Software executes g-code and controls the motion stages through a common controller.

The control hardware consists of:

- Power supply and motion stage controller:

- The electrical and software components consist of:

- Computer: with dedicated control hardware for real-time motion stage control. Uses firewire connection to the motion stage controller.

- Motion stage control software: executes g-code language. Controls the motion stages in real time to allow for smooth motions of all stages.

5.3 Description of Reconfigurable Manufacturing System for Two-Photon Polymerization

The RMS-TPP is reconfigurable to allow it to work with a variety of lasers, as well as substrate and resin tray heights. The system also adapts to a range of lasers, both amplified and oscillator-only, and beam diameters with interchangeable telescope elements. Figures 5.4 to 5.6 are computer renderings of the RMS-TPP.

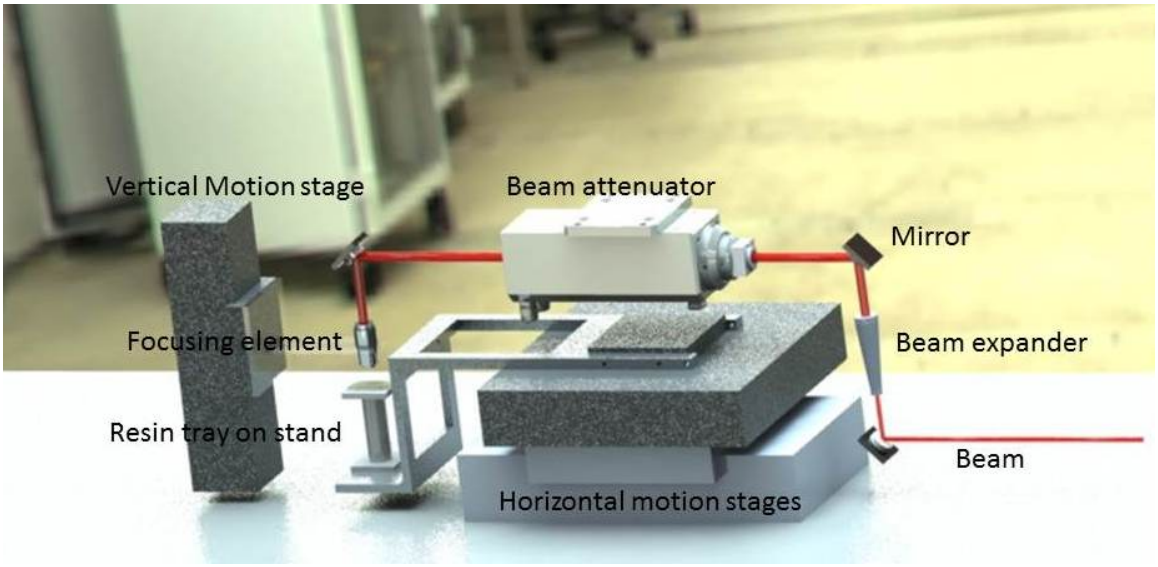

Figure 5.4: Prototype manufacturing system with labels

The beam attenuator controls the power on the focusing element. The motion stages control the speed of the focal point. The beam expander and focusing element control the focal spot size. And the resin sensitivity is set by the composition and preconditioning of the mixture used.

Figure 5.5: Prototype manufacturing system front view with case

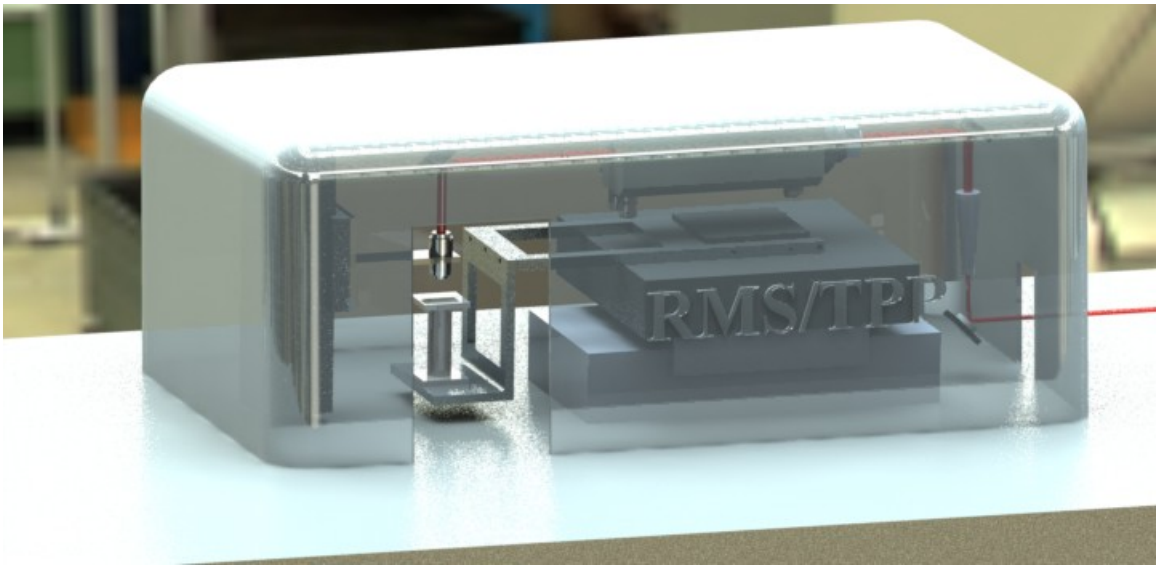

Figure 5.6: Prototype manufacturing system with clear housing

CHAPTER VI

Conclusions and Future Work

6.1 Research Summary and Conclusions

The objective of this research was to analyze and develop a model for the laser-resin interaction and voxel formation during two-photon polymerization. The voxel formed varies with the process parameters used during two-photon polymerization: laser power, focusing element, resin sensitivity, and exposure time. The model prediction shows that with increasing power more resin is polymerized and a larger voxel is formed. This larger voxel also changes in aspect ratio as higher powers are used. The model also predicts that the most sensitive parameters during two-photon polymerization are the laser power and the resin sensitivity, both causing about a 1.5% change in the voxel formed for a 1% change in either process parameter.

This model was then experimentally validated. The experimental validation took place using both amplified and oscillator-only femtosecond pulsed infra-red lasers, as well as a variety of optical elements, and resins. The optical elements used were both singlet lenses and compound microscope objects. The resins used ranged from commercially available photoresists to specially formulated resins comprised of photoinitator molecules and free radical polymerizable monomers. With the model formulated and two-photon polymerization shown as a viable and potentially useful tool for manufacturing polymeric microdevices, the development of a reconfigurable manufacturing system was presented.

From the analytic model formulation a model for analytically determining the volume and shape of a voxel formed by two-photon polymerization has been developed. It takes into account the effects of several process parameters including beam power, lens numerical aperture (NA), resin sensitivity, and exposure time during the process. The analysis shows that the voxel volume is most sensitive to changes in the beam power at the focal point and the polymerization rate of the resin, and less sensitive to changes in beam diameter. It also shows that the voxel size increases with both the beam power and exposure time. Two-photon polymerization experiments demonstrated the validity of the model.

From the methodology for two-photon polymerization a methodology is developed for creating micro-devices by two-photon polymerization, starting from design of the device using a CAD package through the optimization process for the laser path, to the actual control of the motion stages to produce the design. With this methodology it is possible to design and determine the process parameters for creating the micro-device by two-photon polymerization in an optimal fashion. It has also been shown that significant savings in processing time and removal of unwanted features can be achieved using the optimization algorithm developed. Following the presented methodology allows any three-dimensional micro-device within the operational limits of the manufacturing system to be created.

From the holographic polymerization model, holography is investigated as a potential tool for enhancing productivity of the two-photon polymerization process. It is shown that holographic optical elements represent a viable tool for creating complex devices by two-photon polymerization. The significance of this work is the potential for large scale application of the two-photon polymerization methodology.

From the description of the RMS-TPP hardware, the prototype reconfigurable manufacturing system is presented and the process for managing the hardware with the software methodology developed in previous chapters is shown. This prototype manufacturing system has been shown to work for both amplified and oscillator only laser systems. The reconfigurable manufacturing system (RMS-TPP) was designed as a closed box solution

to manufacturing devices by two-photon polymerization. The RMS-TPP system operates using similar machine control code to other machines found on the factory floor (g-code), and is reconfigurable by changing optical elements to allow the same manufacturing system to adapt to a variety of micro-device designs. The RMS-TPP is also compatible with both amplified and oscillator-only pulsed laser systems.

With the work presented in this thesis the foundation is laid to use the RMS-TPP as a functional tool for future commercial and research applications.

6.2 Areas of Future Research

There are a variety of potential areas of future research in the field of two-photon polymerization and adapting the process to more commercial fabrication applications. Because of the compatibility of two-photon polymerization with commercial photoresists, using two-photon polymerization to replace several steps in the MEMS fabrication process is an attractive option. For this application the RMS-TPP can be reconfigured to work with the different substrate materials and optical elements used that are compatible with photoresist type and layer thickness.

With continually increasing laser powers, two-photon polymerization could be compatible with more optical elements, thus increasing the application possibilities and sizes of devices that are possible using two-photon polymerization . Again, the principles used in the RMS-TPP design allow the system to be compatible with future developments in lasers and optical elements.

Applying the RMS-TPP directly to commercial applications is a promising avenue for future work as this would bring the work of lab based study to a wider range of applications. Increasing the use of two-photon polymerization as a tool for micro-device fabrication would further expose this topic to future research ideas that currently, without these commercial applications, are yet unknown.

APPENDICES

APPENDIX A

Voxel Size Appendix

This section provides the detailed derivation of the model equations used for the voxel size analysis. The derivation begins with electromagnetic wave equations as described by *Guenther* (1990).

Beginning with the paraxial wave equation, *Guenther* (1990):

$$\frac{\partial^2 \Psi}{\partial x^2} + \frac{\partial^2 \Psi}{\partial y^2} - 2ik\frac{\partial \Psi}{\partial z} = 0 \tag{A.1}$$

And assuming a solution to this equation has the form:

$$\Psi = e^{-iQ(z)(x^2+y^2)} e^{-iP(z)} \tag{A.2}$$

Where $Q(z)$ is the complex variable associated with the reciprocal of the Gaussian width, and $P(z)$ contains the wave phase information, *Guenther* (1990).

This solution -limited to Gaussian beams with circular cross-sections, TEM_{00} is used to derive the beam parameters used in the laser-resin polymerization model.

Substituting equation (A.2) into equation (A.1) yields:

$$-4(x^2+y^2)Q^2 - 4iQ - 2k\frac{\partial P}{\partial z} - 2k(x^2+y^2)\frac{\partial Q}{\partial z} = 0 \tag{A.3}$$

Let:

$$Q = \frac{k}{2q} \tag{A.4}$$

$$q = \frac{k}{2Q} \tag{A.5}$$

where q is the desired Gaussian beam width. And we may write:

$$Q(z) = \frac{k}{2(q_0 + z)} \tag{A.6}$$

Considering the amplitude of Ψ at $z = 0$ (the focal position) yields:

$$\Psi_0 = e^{\left[-\frac{k(x^2+y^2)}{2q_0}\right]} = e^{\left[-\frac{x^2+y^2}{w_f^2}\right]} \tag{A.7}$$

Equation (A.7) is a Gaussian function.

When we define the minimum beam waist at this focal position, $z = 0$:

$$w_f^2 \equiv \frac{2q_0}{k} \tag{A.8}$$

Yielding a confocal parameter of:

$$q_0 \equiv \frac{kw_f^2}{2} = \frac{\pi w_f^2}{\lambda} \tag{A.9}$$

Ψ now defines the Gaussian beam in terms of its components, *Guenther* (1990):

$$\Psi = \underbrace{\left(\frac{w_f}{w(z)}\right) e^{\left(-\frac{(x^2+y^2)}{w(z)^2}\right)}}_{\text{amplitude}} \underbrace{e^{\left(-ik\frac{(x^2+y^2)}{2R(z)}\right)}}_{\text{paraxial wave}} \underbrace{e^{(-i\phi(z))}}_{\text{phase}} \tag{A.10}$$

Converting to a radial distance since the intensity distribution is equal for all angular directions gives $r^2 = x^2 + y^2$.

The amplitude term of Ψ is used to model the intensity distribution of the Gaussian beam and to determine the intensity of the beam at any position along its path and a radial distance (r) from the center of the beam.

The effect of an optical element on the Gaussian beam parameters can be calculated using the *ABCD* law to relate the input and output parameters of an optical element, figure A.1.

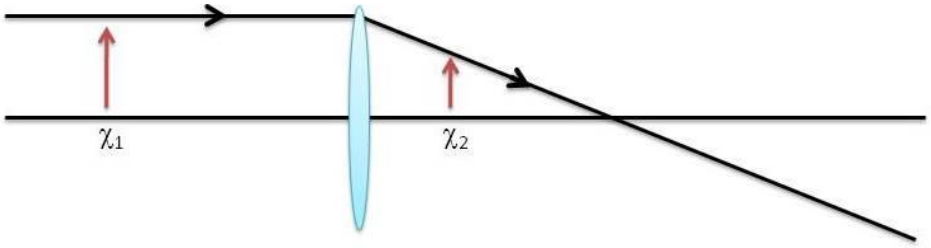

Figure A.1: Effect of a thin lens on a collimated beam.

Using the principle planes theory for a thin lens the *ABCD* matrix formulation can be used to determine the beam waist of a focused Gaussian beam.

$$\begin{pmatrix} x_2 \\ \gamma_2 \end{pmatrix} = \begin{pmatrix} A & B \\ C & D \end{pmatrix} \begin{pmatrix} x_1 \\ \gamma_1 \end{pmatrix} = \begin{pmatrix} 1 & 0 \\ -1/f & 1 \end{pmatrix} \begin{pmatrix} x_1 \\ \gamma_1 \end{pmatrix} \tag{A.11}$$

$$w_f^2 = \frac{\frac{D^2}{4}}{\left[1+\left(\frac{\pi D^2}{4\lambda f}\right)^2\right]} \tag{A.12}$$

$$\frac{1}{q_1} = \frac{1}{R_1} - \frac{i\lambda}{\pi w^2} = \frac{1}{\infty} - \frac{i\lambda}{\pi\left(\frac{D}{2}\right)^2} = 0 - \frac{4i\lambda}{\pi D^2} \tag{A.13}$$

$$\frac{1}{q_1} = -\frac{4i\lambda}{\pi D^2} \tag{A.14}$$

$$q_2 = \frac{Aq_1 + B}{Cq_1 + D} = \frac{1\left(-\frac{\pi D^2}{4i\lambda}\right) + 0}{\left(\frac{-1}{f}\right)\left(-\frac{\pi D^2}{4i\lambda}\right) + 1} \tag{A.15}$$

$$\frac{1}{q_1} = \frac{1}{R} - \frac{i\lambda}{\pi w^2} \Rightarrow \frac{1}{R} = \frac{1}{q} + \frac{i\lambda}{\pi w^2} \tag{A.16}$$

$$\frac{1}{R_2} = -\frac{i\lambda}{\pi\left(\frac{D}{2}\right)^2} - \frac{1}{f} + \frac{i\lambda}{\pi w^2} = -\frac{1}{f} \tag{A.17}$$

The focal spot size w_f can be derived as:

$$w_f^2 = \frac{\frac{D^2}{4}}{\left[1 + \left(\frac{\pi D^2}{4\lambda f}\right)^2\right]} \tag{A.18}$$

The relation of the beam power (P) to the beam intensity (I) at the focal point is derived by integrating the Gaussian beam intensity profile A.19:

$$I(r) = I_0 e^{\left(-\frac{r^2}{w_f^2}\right)} \tag{A.19}$$

$$P = I_f \int_{r=0}^{\infty} \int_{\theta=0}^{2\pi} e^{\left(-\frac{r^2}{w_f^2}\right)} r d\theta dr \tag{A.20}$$

$$P = 2\pi I_f \int_{r=0}^{\infty} e^{\left(-\frac{r^2}{w_f^2}\right)} r dr \tag{A.21}$$

$$P = \pi I_f \int_{v=0}^{\infty} e^{\left(-\frac{v}{w_f^2}\right)} dv \tag{A.22}$$

$$I_p(z) = \frac{P}{\pi w_f^2 \sqrt{1 + \left(\frac{\lambda z}{w_f^2 \pi}\right)}} \tag{A.23}$$

which can now be used to define the radius of the expect region of polymerization, where the beam intensity is greater than or equal to the threshold intensity for polymerization:

$$r_t(z) = w(z)\sqrt{ln(I_p(z)) - ln(I_t) + ln\left(\frac{w_f}{w(z)}\right)} \tag{A.24}$$

The power required in the focal region for polymerization:

$$P = I_f \int_{-Z_{max}}^{+Z_{max}} \int_{r=0}^{\infty} \int_{\theta=0}^{2\pi} \left[\frac{w_f}{w(z)}\right] e^{\left(-\frac{r^2}{w(z)^2}\right)} r d\theta dr dz \tag{A.25}$$

$$P = 2\pi I_f \int_{-Z_{max}}^{+Z_{max}} \int_{r=0}^{\infty} \left[\frac{w_f}{w(z)}\right] e^{\left(-\frac{r^2}{w(z)^2}\right)} r dr dz \tag{A.26}$$

$$P = \pi I_f \int_{-Z_{max}}^{+Z_{max}} \left[\frac{w_f}{w(z)}\right] e^{\left(-\frac{r^2}{w(z)^2}\right)} dz \tag{A.27}$$

$$P = \pi I_f w_f \int_{-Z_{max}}^{+Z_{max}} w(z) dz \tag{A.28}$$

$$P = \pi I_f w_f \int_{-Z_{max}}^{+Z_{max}} \sqrt{1 + \left(\frac{\lambda z}{w_f^2 \pi}\right)^2} dz \tag{A.29}$$

$$P = z_{max}\sqrt{1 + m^2 z_{max}^2} + \left(\frac{1}{2m}\right)\left(ln(mz_{max} + \sqrt{1 + m^2 z_{max}^2}) - ln(-mz_{max} + \sqrt{1 + m^2 z_{max}^2})\right) \tag{A.30}$$

Where z_{max} is defined length in the direction along the beam (z direction) where the peak intensity equals the threshold intensity for polymerization.

$$z_{max} = \frac{\sqrt{P^2 - I_t^2 w_f^4 \pi^2}}{I_t \lambda} \tag{A.31}$$

$$I(z,r) = \frac{P}{\pi w_f w(z)} \left(\frac{w_f}{w(z)} \right) e^{\left(\frac{-r^2}{w(z)^2} \right)} e^{-\alpha z} \tag{A.32}$$

$$A = \pi r_p(z)^2 \tag{A.33}$$

$$r_p = \sqrt{\frac{A}{\pi}} = \sqrt{\frac{k_p t}{\pi}} \tag{A.34}$$

$$k_p = [I(z,r) - I_t]\, m \tag{A.35}$$

$$r(z,r) = \sqrt{\frac{\left[\frac{P}{\pi w_f w(z)} \left(\frac{w_f}{W(Z)} \right) e^{\left(\frac{-r^2}{w(z)^2} \right)} e^{-\alpha z} - I_t \right] mt}{\pi}} \tag{A.36}$$

where:

$$I_t = I_f e^{\left(-\frac{r_t^2}{w_f^2} \right)} \tag{A.37}$$

APPENDIX B

Derivation of (2.8)

Starting with a more generalized form of equation (2.7), from the Gaussian diffraction as described by *Guenther* (1990):

$$P_f = \pi I_f w_f w(z) \tag{B.1}$$

we get:

$$I_p(z) = \frac{P}{\pi w_f w(z)} \tag{B.2}$$

where $w(z) = w_f$ at $z = 0$.

Combining with the Gaussian diffraction as a function of position (z), *Guenther* (1990):

$$w(z) = w_f \sqrt{1 + \left(\frac{\lambda z}{w_f^2 \pi}\right)^2} \tag{B.3}$$

gives the peak intensity as a function of z:

$$I_p(z) = \frac{P}{\pi w_f^2 \sqrt{1 + \left(\frac{\lambda z}{\pi w_f^2}\right)^2}} \tag{B.4}$$

APPENDIX C

Derivation of (2.10)

Starting with the equation (2.2), and substituting I_t and r_t, the equation describes the locations where the intensity distribution is equal to the threshold intensity:

$$I_t = \left(\frac{w_f}{w(z)}\right) I_p(z) e^{\left(-\frac{r_t^2(z)}{w_f^2}\right)} \tag{C.1}$$

Taking the natural log of both sides gives:

$$ln(I_t) = ln\left(\left(\frac{w_f}{w(z)}\right) I_p(z) e^{\left(-\frac{r_t^2(z)}{w_f^2}\right)}\right) \tag{C.2}$$

$$\frac{r_t^2(z)}{w_f^2} = ln\left(\frac{w_f}{w(z)}\right) + ln(I_p(z)) - ln(I_t) \tag{C.3}$$

$$r_t(z) = w_f \sqrt{ln(I_p(z)) - ln(I_t) + ln\left(\frac{w_f}{w(z)}\right)} \tag{C.4}$$

APPENDIX D

Derivation of (2.16)

Substituting equation (2.11) into equation (2.15) gives equation (D.1):

$$k_p = \left[\frac{P}{\pi w_f w(z)} \left(\frac{w_f}{w(z)} \right) e^{\left(\frac{-r^2}{w(z)^2} \right)} e^{-\alpha(Z_{max}-z)} - I_t \right] m \tag{D.1}$$

Further substituting into equation (2.14):

$$r_p = \sqrt{\frac{A_0 + k_p t}{\pi}} \tag{D.2}$$

we get:

$$r_p(z,r) = \sqrt{\frac{A_0 + \left[\frac{P}{\pi w_f w(z)} \left(\frac{w_0}{w(z)} \right) e^{\left(\frac{-r^2}{w(z)^2} \right)} e^{-\alpha(Z_{max}-z)} - I_t \right] mt}{\pi}} \tag{D.3}$$

BIBLIOGRAPHY

BIBLIOGRAPHY

Applegate, D. L., R. E. Bixby, V. Chvtal, W. Cook, D. G. Espinoza, M. Goycoolea, and K. Helsgaun (2009), Certification of an optimal tsp tour through 85,900 cities, *Operations Research Letters*, *37*, 11–15.

Awatsuji, Y., Y. Matsuura, T. Shimizu, and T. Kubota (2002), Analysis of imaging characteristics and design of hoe considering light efficiency using the hologram cad tool, *Proceedings of SPIE - Practical Holography XVI and Holographic Materials VIII*, *4659*, 121–128.

Croitoru, C. (1982), An analysis of the greedy algorithm for partially ordered sets, *Discrete Applied Mathematics*, *4*, 113–117.

Davis, K., K. Miura, N. Sugimoto, and K. Hirao (1996), Writing waveguides in glass with a femtosecond laser, *Optical Society of America*, *21*, 1729–1731.

Day, D., M. Gu, and A. Smallridge (1999), Use of two photon excitation for erasable-rewritable three-dimensional bit optical data storage in a photorefractive polymer, *Optical Society of America*, *24*, 948–950.

DeVoe, R., H. Kalweit, and C. Leatherdale (2003), Voxel shapes in two-photon microfabrication, *Multiphoton Absorption and Nonlinear Transmission Processes: Materials, Theory, and Applications*, *4797*, 310–316.

Galajda, P., and P. Ormos (2001), Complex micromachines produced and driven by light, *Applied Physics Letters*, *78*, 249–251.

Glezer, E., M. Milosavljevic, L. Huang, R. Finlay, T. Her, J. Callan, and E. Mazur (1996), Three-dimensional optical storage inside transparent materials, *Optical Society of America*, *21*, 2023–2025.

Goeppert-Mayer, M. (1931), Elementary processes with two-quantum transitions, *Annalen der Physik*, *9*, 273.

Goeppert-Mayer, M., and M. Born (1931), Dynamic lattice theory of crystals, *Handbuch der Physik*, *24*, 623.

Guenther, R. (1990), *Modern Optics*, John Wiley & Sons.

Haines, K. (1966), The analysis and application of hologram interferometry, Ph.D. thesis, University of Michigan.

Hariharan, P. (1996), *Optical Holography*, Cambridge Studies in Modern Optics.

Hariharan, P. (2002), *Basics of Holography*, Cambridge University Press.

Honegger, T., T. Elmberg, K. Berton, and D. Peyrade (2011), Visible microlaser two-photon polymerization in a microfluidic cell: A resist study, *Microelectronic Engineering*, *88*, 2725–2728.

Houbertz, R., J. Schulz, L. Frohlich, G. Domann, and M. Popall (2003), Inorganic-organic hybrid materials for real 3-d sub-μm lithography, *Materials Research Society*, *442*, 194–200.

Jae-Won, C., W. Ryan, and L. Seok-Hee (2009), Fabrication of 3d biocompatible/biodegradable micro-scaffolds using dynamic mask projection microstereolithography, *Journal of Materials Processing Technology*, *209*, 5494–5503.

Kalantari, B., A. Hill, and S. Arora (1985), An algorithm for the traveling salesman problem with pickup and delivery customers, *European Journal of Operation Research*, *22*, 377–386.

Kawata, S., and H. Sun (2003), Two-photon photopolymerization as a tool for making micro-devices, *Applied Surface Science*, *208*, 153–158.

Kawata, S., H. Sun, T. Tanaka, and K. Takada (2001), Finer features for functional microdevices, *Nature*, *412*, 697–698.

Kuebler, S., et al. (2000), Three-dimensional microfabrication using two-photon activated chemistry, *Micro- and Nano-Photonic Materials and Devices*, *3937*, 97–105.

Kuebler, S., et al. (2001), Optimizing two-photon initiators and exposure conditions for three-dimensional lithographic microfabrication, *Journal of Photopolymer Science and Technology*, *14*, 657–668.

Li-Hsin, H., M. Gazell, and C. Shaochen (2008), Projection microfabrication of three-dimensional scaffolds for tissue engineering, *Journal of Manufacturing Science and Engineering - Transactions of the ASME*, *130*, 021,005.

Lindberg, P., J. Leingang, D. Lysaker, S. U. Khan, and J. Li (2010), Comparison and analysis of eight scheduling heuristics for the optimization of energy consumption and makespan in large-scale distributed systems, *Journal of Supercomputing*, *59*, 323–360.

Ma, L., H. Wang, Y. Li, and H. Jin (2012), Partition calculation for zero-order and conjugate image removal in digital in-line holography, *Optics Express*, *20*, 1805–1815.

Marsh, J., and R. Smith (1976), Computer holograms with a desk-top calculator, *American Journal of Physics*, *44*, 774–777.

Maruo, S. (1997), Two photon absorbed photopolymerization for three dimensional microfabrication, Ph.D. thesis, Department of Applied Physics, Osaka University.

Maruo, S., and H. Inoue (2006), Optically driven micropump produced by three-dimensional two-photon microfabrication, *Applied Physics Letters*, *89*, 144,101.

Maruo, S., and S. Kawata (1998), Two photon absorbed near infrared photopolymerization for three dimensional microfabrication, *Journal of Microelectromechanical Systems*, *7*, 411–415.

Misawa, H., and S. Juodkazis (Eds.) (2006), *3D Laser Microfabrication*, Wiley-VCH.

Nakata, Y., T. Okada, and M. Maeda (2004), Generation of uniformly spaced and nano-sized structures by interfered femtosecond laser beams, *Photon Processing in Microelectronics and Photonics III - Proceedings of SPIE*, *5339*, 9–19.

Odian, G. (1970), *Principles of Polymerization*, McGraw-Hill Book Company.

Olson, D. (1989), The elementary plane-wave model for hologram ray tracing, *American Journal of Physics*, *57*, 445–455.

Pavillon, N., C. Arfire, I. Bergond, and C. Depeursinge (2010), Iterative method for zero-order suppression in off-axis digital holography, *Optics Express*, *18*, 15,318–15,331.

Saxby, G. (2004), *Practical Holography*, Institute of Physics Publishing.

Seibel, R. (2002), Manipulation of micro scale particles in an optical trap using interferometry, Ph.D. thesis, University of Akron.

Serbin, J., A. Ovsianikov, and B. Chichkov (2004), Fabrication of woodpile structures by tpp and investigation of their optical properties, *Optics Express*, *12*, 5221–5228.

Sodemann, A. A., and J. R. Mayor (2008), Intelligent tool-path segmentation for improved stability and reduced machining time in micromilling, *Journal of Manufacturing Science and Engineering - Transactions of the ASME*, *130*, 031,121.

Sodemann, A. A., and J. R. Mayor (2011), Experimental evaluation of the variable-feedrate intelligent segmentation method for high-speed, high-precision micromilling, *Journal of Manufacturing Science and Engineering - Transactions of the ASME*, *133*, 021,001.

Sun, H., S. Matsuo, and H. Misawa (1999), Three-dimensional photonic crystal structures achieved with two photon absorption photopolymerization of resin, *Applied Physics Letters*, *74*, 786–788.

Sun, H., T. Kawakami, Y. Xu, J. Ye, S. Matsuo, and H. Misawa (2000), Real three-dimensional microstructures fabricated by photopolymerization of resins through two photon absorption, *Optical Society of America*, *25*, 1110–1112.

Sun, H., K. Takada, and S. Kawata (2001a), Elastic force analysis of functional polymer submicron oscillators, *Applied Physics Letters*, *79*, 3173–3175.

Sun, H., T. Tanaka, and S. Kawata (2002), Three-dimensional focal spot related to two photon excitation, *Applied Physics Letters*, *80*, 3673–3675.

Sun, H., M. Maeda, and K. Takada (2003), Experimental investigation of single voxels for laser nanofabrication via two-photonphotopolymerization, *Applied Physics Letters*, *83*, 819–821.

Sun, H.-B., T. Tanaka, K. Takada, and S. Kawata (2001b), Two-photon photopolymerization and diagnosis of three-dimensional microstructures containing fluorescent dyes, *Applied Physics Letters*, *79*, 1411–1414.

Sviridenko, M. (2000), Worst-case analysis of the greedy algorithm for a generalization of the maximum p-facility location problem, *Operations Research Letters*, *26*, 193–197.

Vest, C. M. (1979), *Holographic Interferometry*, John Wiley & Sons.

Weibel, D., W. DiLuzio, and G. Whitesides (2007), Microfabrication meets microbiology, *Nature Reviews*, *5*, 209–218.

Witzgall, G., R. Vrijen, E. Yablonovitch, V. Doan, and B. Schwartz (1998), Single-shot two-photon exposure of commercial photoresist for the production of three-dimensional structures, *Optics Letters*, *23*, 1745–1747.

Wu, S., J. Serbin, and M. Gu (2006), Two-photon polymerisation for three-dimensional micro-fabrication, *Journal of Photochemistry and Photobiology A: Chemistry*, *1*, 11.

Yamada, A., F. Niikura, and K. Ikuta (2007), Fabrication of biodegradable microdevices toward medical application, *IEEE/ASME International Conference on Advanced Intelligent Mechatronics, AIM*, *1-3*, 1007–1011.

Zhang, W., L.-H. Han, and S. Chen (2010), Integrated two-photon polymerization with nanoimprinting for direct digital nanomanufacturing, *Journal of Manufacturing Science and Engineering*, *132*, 030,907.